SPITFIRE-1

A COOPERATIVE AGREEMENT FOR THE DEVELOPMENT OF
RAPID LOW-COST SUPERPLASTIC FORMING OF ALUMINUM
COOPERATIVE AGREEMENT NUMBER NCCW-0034

PROGRESS REPORT: TWELVE-MONTH DELIVERABLES

MARCH 1, 1995 — MAY 31, 1995

SUBMITTED TO NASA
BY GENERAL MOTORS RESEARCH AND DEVELOPMENT CENTER
NOVEMBER 17, 1995

PRINCIPAL INVESTIGATOR: EDWARD F. RYNTZ
METALLURGY DEPARTMENT, GM RESEARCH AND DEVELOPMENT CENTER
30500 MOUND ROAD (BLDG. 1-6), WARREN, MI 48090-9055
PHONE: (810) 986-1011

BUSINESS CONTACT: DR. M. S. RASHID
METALLURGY DEPARTMENT, GM RESEARCH AND DEVELOPMENT CENTER
30500 MOUND ROAD (BLDG. 1-6), WARREN, MI 48090-9055
PHONE: (810) 986-0949

TABLE OF CONTENTS

ABSTRACT 1

INTRODUCTION 2

TOPIC 1—ALLOY DEVELOPMENT 4

1.1. BASELINE ALLOY PROPERTIES 4

General Motors Research and Development Center 5

1.1.1, 1.1.3, 1.1.5, and 1.1.7 Biaxially formed components from modified superplastic 5000 Al alloys 5

Microstructural Characterization 5

Stress Corrosion Cracking (SCC) Susceptibility Study 5

Superplastic Characterization 6

Accurate Strain Rate Control During Tensile Testing 6

University of Michigan 15

Thermomechanical Processing and Superplasticity of an Al-4.7% Mg Alloy Modified by Cu .. 15

Materials and experimental methods 15

Materials 15

Thermomechanical processing and tensile testing 15

Metallography 15

TEM study 16

Experimental results and discussion 16

Grain growth and grain boundary pinning by second phase particles 16

Superplastic flow and elongation 16

Strain-induced grain growth and cavitation 18

Battelle Pacific Northwest Laboratories 24

1.1.3 Modify Composition of 5000 Al Alloys and Evaluate Structure Property Relationships .. 24

Thermomechanical Treatments 24

Compositional Effects 24

Dispersoids 24

Eutectic Constituents (ECs) 25

TOPIC 2–MANUFACTURING PROCESSES 30

2.1 AND 2.2 BASELINE MANUFACTURING PROCESSES AND RAPID FORMING ALTERNATIVES 30

General Motors Research and Development Center 30

2.1.1.13 Conduct exploratory tests on hybrid forming 30

2.1.2.3 Determine post-SPF mechanical properties 31

2.1.3.2 Establish processing targets for rapid SPF 31

2.1.3.3 Establish post-SPF property targets for rapid SPF 31

2.1.1 - ESTABLISH FORMING PARAMETERS FOR EXISTING MANUFACTURING PROCESSES FOR SUPERPLASTIC ALUMINUM AND 2.1.2 - EVALUATE THE QUALITY OF MANUFACTURED COMPONENTS 31

Pacific Northwest Laboratory 31

Experimental Forming of Alloy 19 31

2.1.1-ESTABLISH FORMING PARAMETERS FOR EXISTING MANUFACTURING PROCESSES FOR SPF ALUMINUM AND 2.2.1-EXPLORE NEW CONCEPTS FOR MAKING SPF ALUMINUM COMPONENTS AT A FASTER RATE. 39

NASA Langley Research Center 39

Rapid Biaxial Forming 39

Part Quality 40

Microstructural Characterization 40
2.3 MULTI-SHEET STRUCTURES 45
Boeing *45*
2.3.2. Explore multi-sheet SPF concepts for automotive structures 45
2.3.2.1 Explore stiffness/crush applications 45
2.3.2.2. Explore part consolidation applications 45
2.3.2.3 Evaluate structural characteristics of multi-sheet components 45
2.3.3. Identify promising multi-sheet structures for further development 46
TOPIC 3-TOOLING & DESIGN **47**
General Motors Research and Development Center *47*
3.2.2.2 Assess changes in the quality of selected SPF tooling materials on extended service;
3.2.2.3 Evaluate viability of tooling concepts for extended service application 47
3.2.3 Identify promising tooling materials and concepts 47
3.3 PART DESIGN AND MANUFACTURING 49
General Motors Research and Development 49
SPF Component Development 49
Web-Stiffened Channel Study 49
SPF Cost Modeling 49
Progress in CAE Development 50
APPENDIX A: TOPIC 1 - ALLOY DEVELOPMENT DELIVERABLES SUMMARY 52
APPENDIX B: TOPIC 2 - MANUFACTURING PROCESSES DELIVERABLES SUMMARY 53
Milestones 53
APPENDIX C: TOPIC 3 - TOOLING & DESIGN DELIVERABLES SUMMARY 54
Milestones 54

ABSTRACT

This is the third progress report on the development of rapid low-cost superplastic forming of aluminum, code-named SPITFIRE-1, satisfying the twelve-month deliverables of the program. The report presents progress on alloy development and thermomechanical processing treatments; current component quality evaluations, feasibility studies of mechanical forming and multi-sheet structures; and tool designs and durability evaluation. Contributions from research partners in the SPITFIRE-1 program are combined under each of the three development topics.

INTRODUCTION

A cooperative agreement was signed in May 1994 between General Motors Corporation (GM) and the National Aeronautic and Space Administration (NASA) for a one-year collaborative research and development effort to develop and deploy an advanced light metal forming technology known as rapid low-cost superplastic forming (SPF) of aluminum. Code-named SPITFIRE-1, this is the first part of a proposed 5-year collaborative effort between GM and NASA.

The focus of this cooperative agreement is to advance aluminum SPF technology from the low-volume, high-cost applications of the aerospace industry to the high-volume, low-cost requirements of the automotive industry. This would benefit both GM and NASA by decreasing their manufacturing costs. Such a shift requires developing SPF technology in three areas: low-cost aluminum alloys, high-rate forming processes, and durable, low-cost tooling with an attendant computer-aided design process. These three development areas represent the major effort of the project.

This report describes progress made during the tenth through twelfth months of this project by GM and its partners: NASA Langley Research Center (LaRC), Kaiser Aluminum & Chemical Corporation Center for Technology (KCFT), Boeing Defense and Space Group (BOE), Battelle Pacific Northwest Laboratories (PNL), the University of Michigan (UM) and Washington State University (WSU).

The report satisfies the twelve-month deliverables of the SPITFIRE-1 program. The individual deliverables for each research partner are combined into a single deliverable under the three major development areas. For the convenience of the reviewers, copies of the original Deliverables Summaries are appended to this report. The four-month and nine-month deliverables were reported in papers submitted January 9, 1995 and July 28, 1995, respectively. A final report summarizing the year's work will be submitted shortly.

ABBREVIATIONS USED IN THIS REPORT

BOE	Boeing Defense and Space Group
GM	General Motors
GM R&D	General Motors Research and Development Center
KCFT	Kaiser Center for Technology
LaRC	NASA Langley Research Center
PNL	Battelle Pacific Northwest Laboratories
UM	University of Michigan
WSU	Washington State University
CBC	chemically bonded ceramics
CDR	continuous dynamic recrystallization
CHS	cross-head speed
CODF	crystallite orientation distribution functions
DDP	Dialog Decision Process
DEGG	deformation-enhanced grain growth
DLC	diamond-like carbon
EC	eutectic constituents
EM	experimental mechanics
LBW	laser beam welding
MMC	metal matrix composites
NC	numerical control
PM	powder metallurgy
SEM	scanning electron microscopy
SGG	static grain growth
SPF	superplastic forming
TEM	transmission electron microscopy
TMA	thermomechanical analyzer
TMP	thermomechanical processing

TOPIC 1—ALLOY DEVELOPMENT

STATEMENT OF WORK

The purpose of this effort is to develop low-cost rapid forming superplastic aluminum that will be evaluated in pilot production trials for automotive SPF components. The alloy development study conducted under SPITFIRE-1 showed that the addition of Cu or Mn to the base 5083 aluminum alloy refined the grain size, leading to enhanced superplastic properties. In SPITFIRE-2, these alloy variants will be further refined and studied to meet the target properties established earlier in the program. Mechanical properties, component forming and post-forming properties will be evaluated. Also, the alloy production process, including thermomechanical processing (TMP) optimization to reduce production cost, will be investigated during SPITFIRE-2. After identifying preferred compositions and production processing, the most promising alloy will be manufactured into production coils for verification during SPITFIRE-3. Components will be produced from these coils in SPITFIRE-4, and the process and component performance will be assessed.

1.1. BASELINE ALLOY PROPERTIES

The effort to identify a single aluminum alloy with enhanced superplastic forming properties continued through the final months of SPITFIRE-1 and will continue during the first part of SPITFIRE-2. Based on data presented at a June 8-9, 1995 program review at NASA-LaRC, six alloy variants were identified for intensive study. Final selection of one or possibly two alloys for processing into a production coil by the end of SPITFIRE-2 is targeted for September 1995. The six alloys that are being evaluated for final selection in subsequent productionizing studies are:

Identification Number	Modification to a nominal 5083 alloy composition		
	Cu	Zr	Mn
K-14	—	—	1.1
K-15	0.4	0.2	0.7
K-16	0.8	0.2	0.7
K-17	—	0.2	1.1
K-24	0.6	—	0.7
K-25	0.6	0.2	0.7

Evaluation of these alloys will consist of tensile tests (GMR&D), forming of a "butter" tray (PNL), and forming of a webbed-reinforced rail (LaRC). The following information was developed during this reporting period and led to the selection of the above six experimental alloys for final evaluation.

General Motors Research and Development Center

1.1.1, 1.1.3, 1.1.5, and 1.1.7 Biaxially formed components from modified superplastic 5000 Al alloys

This section describes information developed under Task 1.1—Baseline Alloy Properties. General Motors Research and Development Center (R&D) is investigating Cu/Zr modified 5083 aluminum alloys produced by Kaiser Center for Technology (KCFT) in order to understand the effect of Cu and/or Zr additions to Al-5% Mg alloys on enhancing superplastic properties. The chemical compositions and grain size of the six alloys that were evaluated during this period are listed in Table 1.

Microstructural Characterization

Grain size measurements on the modified 5083 aluminum alloys listed in Table 1 were performed in a Princeton Gamma Tech image analyzer using ASTM standard E112. Similar grain sizes were found in all alloys containing Zr (5.9 to 6.9 μm), but the grain size of alloy 24 without Zr was a little larger (7.8 μm).

In order to better understand the micromechanical role and behavior of specific precipitates, as-rolled sheets (2 mm thick) of four modified alloys exhibiting better superplastic properties (alloys 15, 16, 24, and 25) were examined by transmission electron microscopy (TEM). To reveal the grain structure, samples received a solutionizing treatment at 535°C for 15 minutes followed by water quenching and aging at 150°C for two hours.

The TEM micrographs in Figure 1, all taken at the same magnification, show the general microstrucure of four alloys. The grain size of all alloys looks similar but the grains in alloys 24 and 25 seem more equiaxed. The size and distribution of precipitates in alloy 16 are less uniform than other alloys, while precipitates in alloy 15 look much coarser. Also, spherical Cu particles larger than one micron, such as the one indicated with an arrow in alloy 15, are occasionally observed in all alloys.

These modified alloys contain several different types of coarse and fine precipitates. Table 2 lists the sizes, preferential sites, and characteristics of those precipitates. Grain boundaries seem to be the preferential sites for fine Al-Mg-Cu particles. Figure 2, taken from alloy 16, reveals the grain boundary network of those fine precipitates. They are, however, depleted near the grain boundary area, which may induce intergranular corrosion due to the difference in electrochemical potential.

The TEM micrograph of alloy K-24 in Figure 3 clearly illustrates coarse Al-Mg-Cu particles pinning high angle grain boundaries. Another Cu-containing precipitate, consisting of $Al_x(MgMnCrCu)_y$ compounds, is located along the grain boundaries and also inhibits the motion of the grain boundary. Such a pinning action at the grain boundary by certain precipitates enhances the grain refinement, resulting in better superplastic properties. The role of boundary precipitates during superplastic forming will be further investigated.

Stress Corrosion Cracking (SCC) Susceptibility Study

It is known that aluminum alloys containing more than 3% Mg are susceptible to SCC. Since the modified 5083 aluminum alloys developed under SPITFIRE-1 contain ~5% Mg, it is of great interest to evaluate stress corrosion properties of these alloys.

Specimens were machined (12mm gage width) from the rolled and superplastically formed sheets of modified alloys, some commercial SPF 5083 and 2004 alloys, and AA5754 alloy. Forty samples in all were sensitized at 165°C for 0, 24, or 168 hours, assembled in spring loaded (~140 kg) tension fixtures, and placed inside the Q-Fog Model CCT 600 Cyclic Corrosion Tester. For simulating a real-world automotive environment, the GM 9540 P Method B test, involving cyclic spray and dry-off, was selected.

Samples exposed more than 60 days have not failed, but heavily corroded surfaces have been observed in the specimens of the 2004 alloys, containing a nominal 6% copper. This experiment will be continued for 90 days. Additional modified 5083 aluminum alloys will also be tested for SCC at GM Corrosion Engineering Facilities.

Superplastic Characterization

Initial investigation of the Cu/Zr modified 5083 alloys, conducted during the past period, established general trends of dependence of uniaxial tensile elongation on the alloy composition, the test conditions, and the specimen orientation. Of the six alloys in Table 1, four alloys (K-15, -16, -24, and -25) were chosen for further investigation to select an alloy for processing into a production coil.

Step strain rate tests were conducted to obtain the optimum superplastic strain rate and the strain rate sensitivity index m for the alloys. The log stress-log strain rate plot and the corresponding m-log strain rate plot for alloy K-16 (0.8%Cu-0.2%Zr) are shown in Figure 4. This alloy exhibits an optimum SPF strain rate of $1x10^{-3}s^{-1}$ with a maximum m value of 0.7. In contrast to this modified alloy, the base SPF grade 5083 alloy has been shown to exhibit an optimum SPF strain rate of about $4x10^{-4}s^{-1}$ with an m value of about 0.6.

Uniaxial tensile tests were conducted at constant strain rate from $5x10^{-4}$ to $3x10^{-2}s^{-1}$ at 500°C, 525°C, and 550°C. While most tests were conducted on specimens cut parallel to the sheet rolling direction, some tests were conducted along the transverse direction as well. Table 3 gives tensile elongation results. Significant anisotropy in tensile elongation was observed between the rolling and the transverse directions in alloys K-15, K-16, and K-24. Tensile elongations for the four alloys are plotted as a function of strain rate at 550°C in Figure 5. Tensile elongation decreases sharply with increasing strain rate for all the alloys. At strain rate of $5x10^{-4}s^{-1}$ alloy K-16 has the highest tensile elongation. However, at strain rates greater than $1x10^{-3}s^{-1}$, K-15 and K-24 show significantly higher tensile elongations than either K-16 or K-25. The effect of test temperature on the tensile elongation-strain rate plot for alloys K-15 and K-24 is shown in Figure 6. At 550°C, tensile elongation decreases sharply with increasing strain rate. However, at 500°C, the strain rate has little effect on tensile elongation. While lowering the test temperature from 550°C to 500°C sharply decreases tensile elongation at $1x10^{-1}s^{-1}$, it significantly increases tensile elongation at $1x10^{-2}s^{-1}$. Alloy K-24, at 500°C and $1x10^{-1}s^{-1}$, exhibits a tensile elongation of 230%, which is very encouraging for SPF forming of actual aluminum parts.

Accurate Strain Rate Control During Tensile Testing

During uniaxial superplastic testing, metal flow from the grip to the gage section of the tensile specimen alters the strain rate in the gage section. An approach of eliminating the metal flow to the gage section by strengthening the grip sections with welded aluminum tabs was investigated during the third quarter. This is a viable approach for maintaining nearly constant

strain rate in 1.27mm gage tensile specimens using the "theoretical" (exponentially increasing) cross-head displacement history.

The University of Michigan has modeled the metal flow in 1.27mm gage tensile specimens, and proposed to control cross-head speed with a corrected displacement history, which compensates for the metal flow from the grip to the gage. This approach was evaluated against simple cross-head displacement options, namely, exponentially increasing cross-head speed (CHS) and constant CHS. Three tensile tests were conducted at 550°C with an intended strain rate of $3x10^{-3}s^{-1}$. Alloy K-15 was used for the study. The three different cross-head displacement histories employed are shown in Figure 7. The first test used the theoretical, exponentially increasing displacement history (no correction for metal flow). The second test used the "corrected" displacement history based on the UM model. The third test used the initial CHS of the second test and maintained a constant CHS through the entire test. Note that the constant CHS used in the third test is not simply the theoretical 1.27mm gage length, but one corrected for the initial rate of metal flow from the grip. The stress-true strain plots for the three tests are shown in Figure 8. Compared to the "Modeled" plot (second test), the "Exp." plot (first test) initially shows lower flow stress values due to lower than intended strain rate in the gage section during the early part of the test. At higher strain levels (greater than 0.6), however, it shows higher flow stress because of underestimation of gage cross-sectional area used in calculating the flow stress. The "Modeled" plot exhibits a more realistic stress-strain plot. In spite of the different nature of the stress-strain plots, the "Exp." and the "Modeled" tests exhibit about the same strain to failure. It is concluded that for alloy selection purposes, where tensile elongation is the main criterion for selection, the "Exp." displacement history is as good as the "Modeled" displacement history. The stress-strain plot for the "Constant CHS" test nearly coincides with the plot for the "Modeled" test up to the point of instability (strain=0.6), beyond which the "Constant CHS" plot shows lowered flow stress values than the "Modeled" plot, indicative of falling strain rate in the former case. Since the current constitutive-behavior modeling is accurate only up to the point of instability, accurate stress-strain data for constitutive equations can be obtained from either the "Modeled" test or the "Constant CHS" test.

Table 1. Cu and Zr Modified 5083 Alloy Sheets

Alloy	Composition		Grain Size, μm
	Cu	Zr	
K-15	0.4	0.2	6.9
K-16	0.8	0.2	6.6
K-22	0.2	0.2	—
K-23	0.2	0.4	6.5
K-24	0.6	—	7.8
K-25	0.6	0.2	5.9

Table 2. Characteristics of Precipitates in Modified Alloys.

Precipitates	Size	Shape	Location	Remarks
Al_3Zr	300~500 Å	spherical	matrix	uniform distribution
Al_6Mn	300~800 Å	spherical	matrix	uniform distribution
	0.2~0.4μm	rod	matrix	uniform distribution
$Al_x(MgMnCrCu)_y$	0.3~0.5μm	twinning, facetting	matrix	
			grain boundary	pinning grain boundary
Al-Mg-Cu	0.3~0.8μm	spherical	grain boundary	pinning grain boundary
	200~400 Å	spherical	grain boundary	grain boundary network

Table 3. Constant Strain Rate Test Results.

Alloy	Additions		Temp	Strain Rate	Orientation	Elongation
	Cu	Zr	(°C)	(s^{-1})		(%)
K-15	0.4	0.2	550	$1x10^{-3}$	L	495
				$1x10^{-3}$		504
				$1x10^{-3}$	T	310
				$3x10^{-3}$	L	295
				$1x10^{-2}$	L	174
				$3x10^{-2}$	L	93
			525	$1x10^{-3}$	L	292
			500	$1x10^{-3}$	L	232
				$1x10^{-2}$	L	215
K-16	0.8	0.2	550	$5x10^{-4}$	L	675
				$1x10^{-3}$	L	530
				$1x10^{-3}$	T	335
				$5x10^{-3}$	L	135
				$1x10^{-2}$	L	77
			500	$1x10^{-3}$	L	275
K-24	0.6	—	550	$1x10^{-3}$	L	475
				$1x10^{-3}$	T	370
				$3x10^{-3}$	L	260
				$1x10^{-2}$	L	138
			525	$1x10^{-3}$	L	316
			500	$1x10^{-3}$	L	289
				$1x10^{-2}$	L	231
K-25	0.6	0.2	550	$1x10^{-3}$	L	400
				$1x10^{-3}$	T	400
				$1x10^{-2}$	L	93
			525	$1x10^{-3}$	L	332
			500	$1x10^{-3}$	L	255
				$1x10^{-2}$	L	165

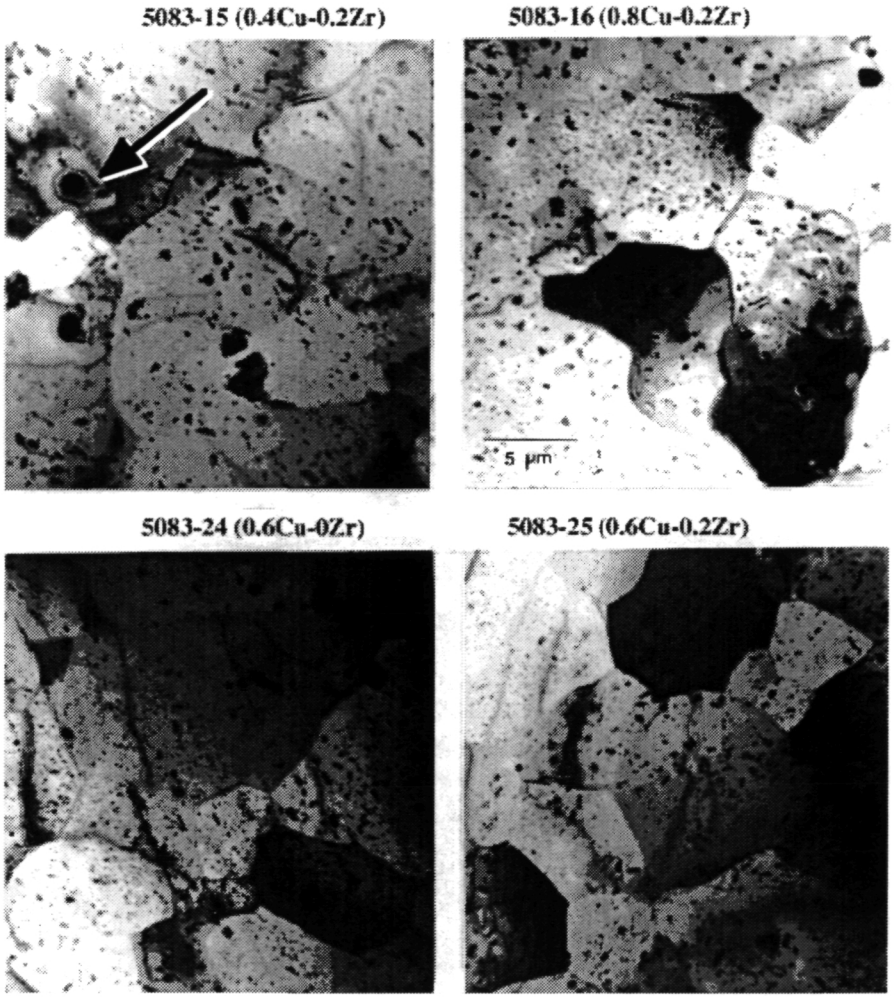

Figure 1. Modified 5083 Alloys (As-Rolled and Heat-Treated). Arrow (upper left) indicates spherical Cu particle larger than one micron in 5083-15 sample.

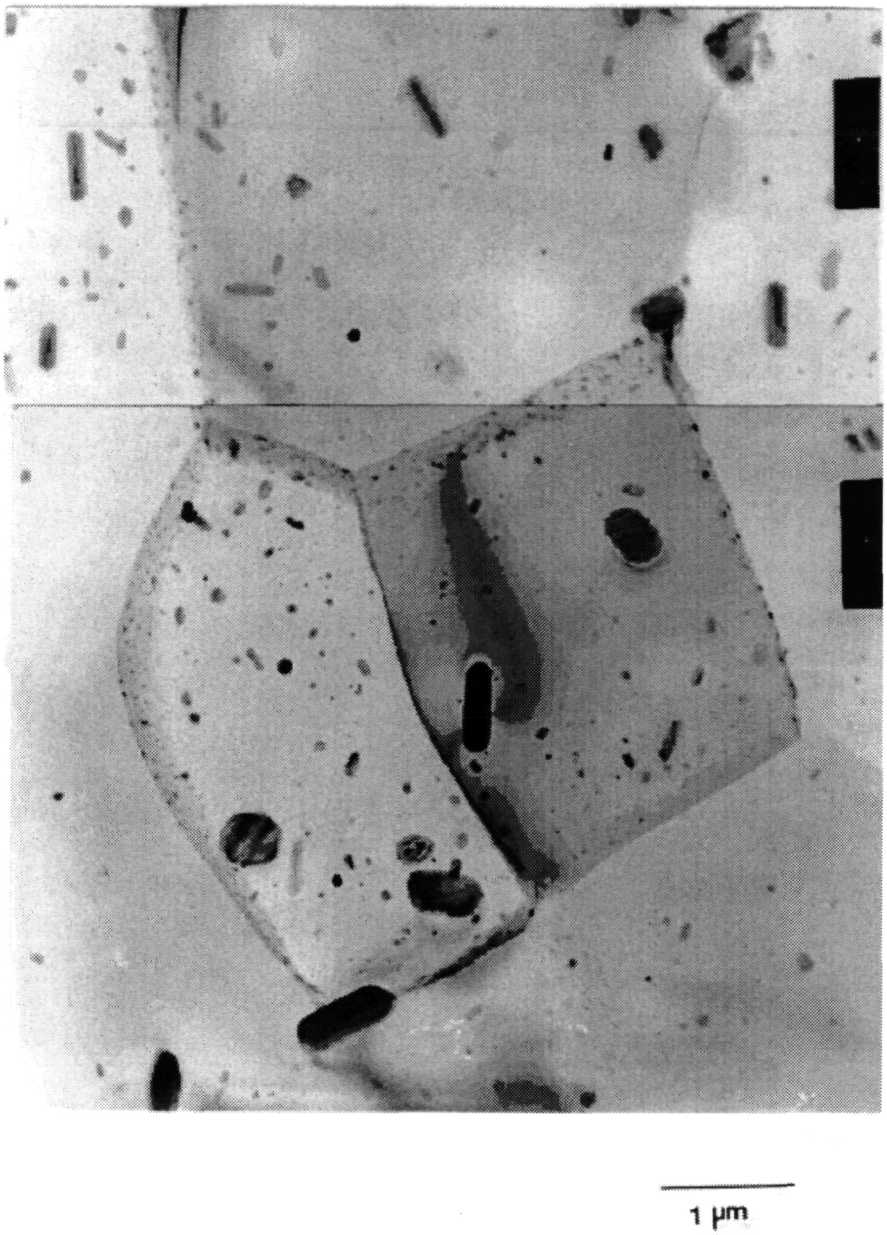

Figure 2. Grain boundary precipitates in alloy K-16 (0.8Cu-0.2Zr)

Figure 3. Grain boundary precipitates in alloy K-24 (0.6Cu-0Zr)

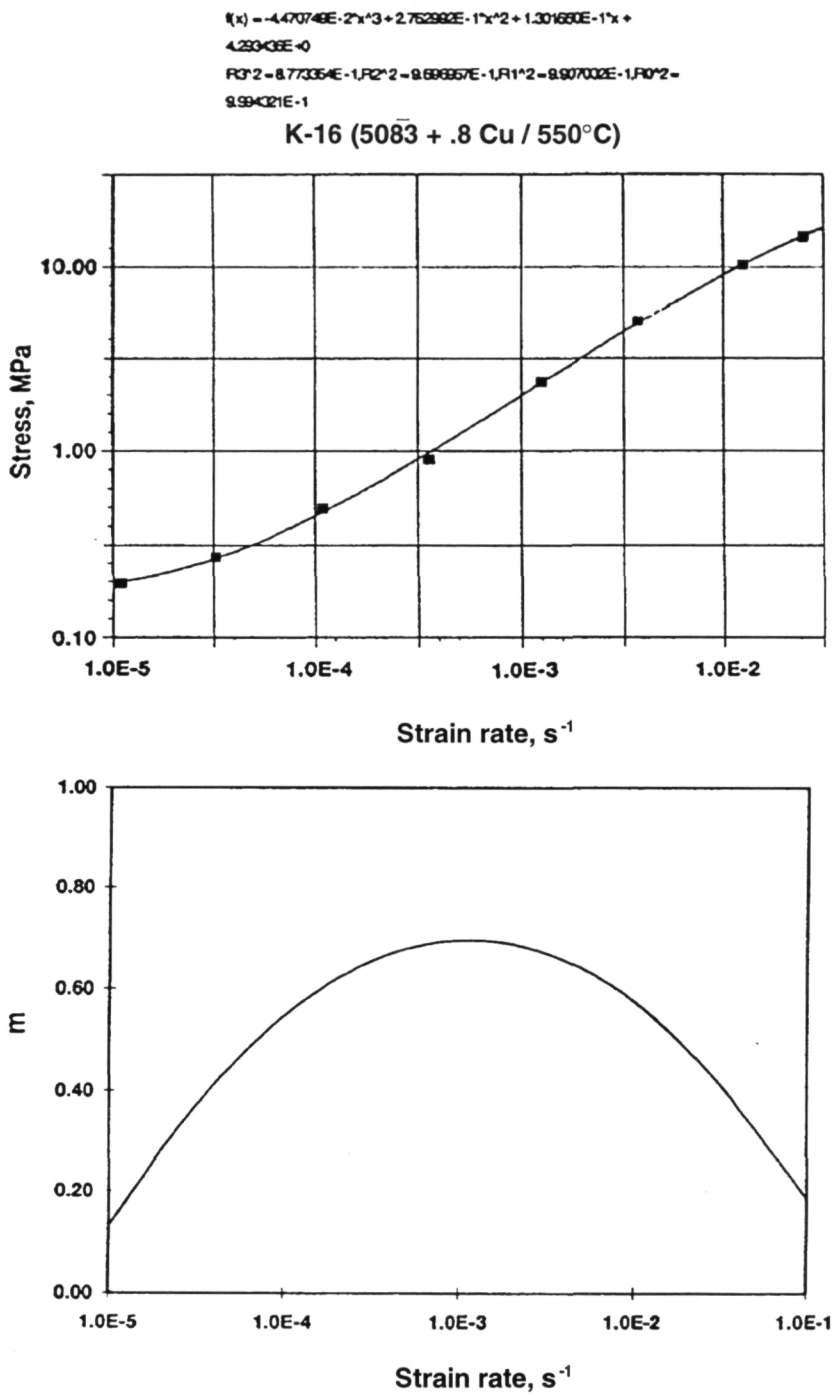

Figure 4. Log stress-log strain rate and m-log strain for alloy K-16 (0.8Cu-0.2Zr).

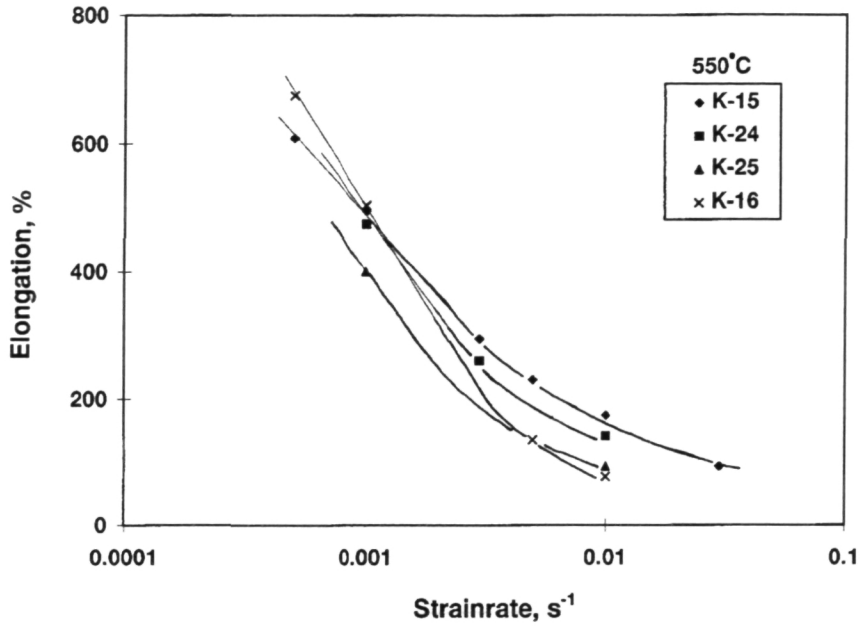

Figure 5. Tensile elongation as a function of strain rate for modified alloys.

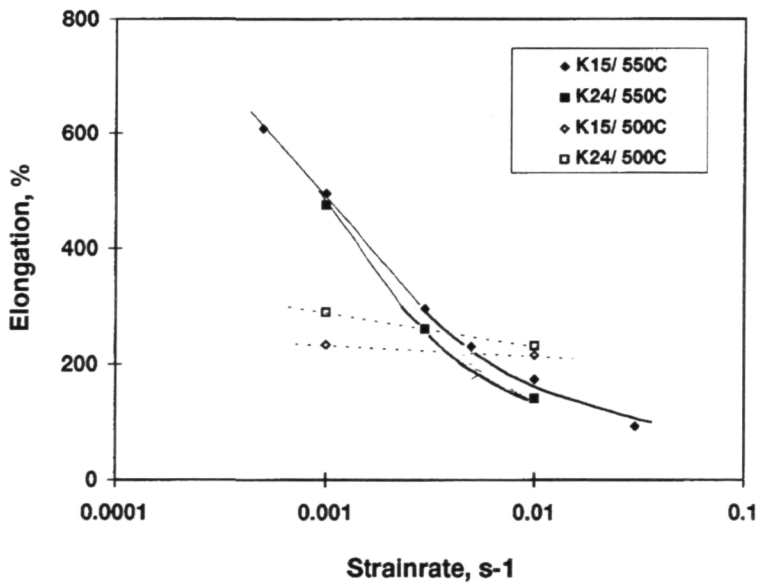

Figure 6. Effect of test temperature on tensile elongation-strain rate for modified alloys.

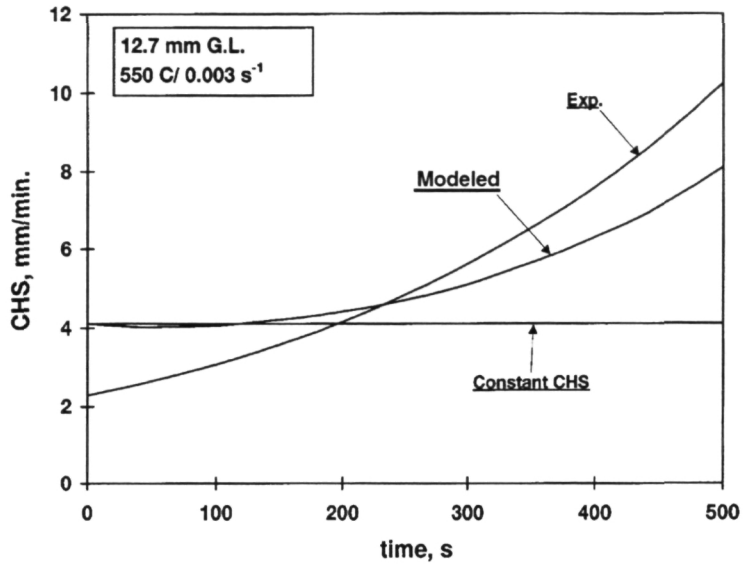

Figure 7. Three different cross-head displacement histories: "Exp." (exponentially increasing, no correction for metal flow), "Modeled" (UM model compensates for metal flow from grip to gage), and "Constant CHS" (corrected for initial rate of metal flow from grip).

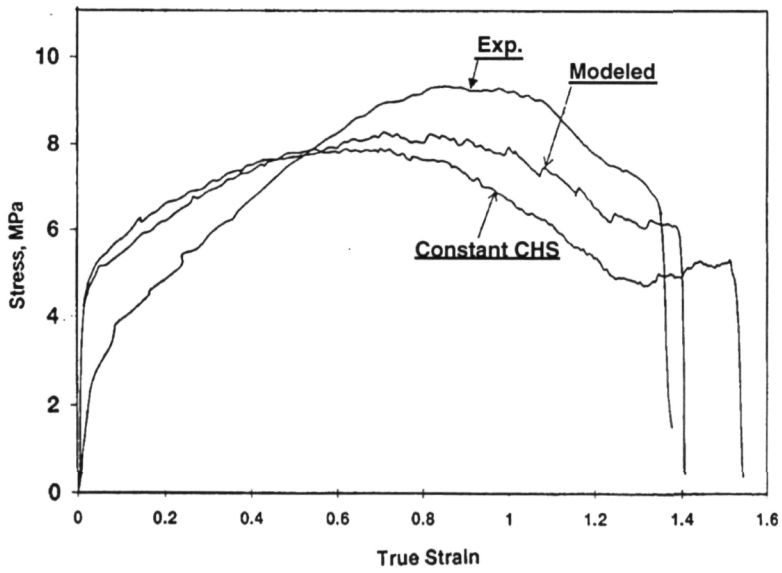

Figure 8. True stress-true strain plot for exponentially increasing, modeled, and constant cross-head displacement histories.

University of Michigan

Thermomechanical Processing and Superplasticity of an Al-4.7% Mg Alloy Modified by Cu

Work in SPITFIRE-1 has shown that commercial Al-4.7% Mg alloy (AA5083), when modified with Cu, generally shows superior superplastic properties. However, the effect of TMP on grain size and cavitation behavior needs to be studied in order to produce the best possible microstructure for forming superplastic parts. The role played by Cu in these materials during superplastic deformation is of primary technical interest. Understanding the role of Cu may provide useful knowledge in optimizing superplastic properties for this new family of alloys.

This section of the report summarizes the results of grain growth, uniaxial testing propeties and cavitation behavior on alloys K-15 and K-16. This work supports the effort ongoing at GM R&D on these same Cu-containing alloys.

Materials and experimental methods.

Materials

Two Al-4.7% Mg alloys containing different amounts of Cu, supplied by Kaiser Center for Technology and designated as K-15 and K-16, were used in the present study. The chemical compositions, in weight percentage, are as follows:

Alloy 15: Al-4.75Mg-0.8Mn-0.4Cu-0.2Cr-0.2Zr

Alloy 16: Al-4.75Mg-0.8Mn-0.8Cu-0.2Cr-0.2Zr

The materials were received as both cast blocks and also cold rolled to 10.3mm thick plates, and flash annealed at 500°C for 10 minutes.

Thermomechanical processing and tensile testing

The thermomechanical processing schedule for the as-received materials is summarized in Figure 9. Prior studies had indicated that these treatments provided a good degree of superplasticity in these alloys.

Homogenization and aging treatments were carried out in an air circulating furnace. The static annealing was performed in a salt bath. Quenching in water was performed after each of these heat treatments.

Tensile tests were conducted on a 4505 Instron machine controlled by a microcomputer to achieve constant strain rate. The details of this part of the experiment have been described in the first SPITFIRE-1 progress report.

Samples removed from the tensile specimens at about 0.635mm away from the fracture surface were used for grain size and cavity density measurement.

Metallography

Samples were mechanically polished then etched with Graf Sergent (15.5ml HNO_3, 0.5ml HF, 3g Cr_2O_3 and 84ml water) reagent. Aging treatment, preferably at 150°C for 24 hours or longer, depending on the grain size, proved to be essential to successfully reveal the grain structure. Grain size was measured by the linear intercept method. The grain size data represent average values determined by the following relationship:

$$d = \sqrt[3]{d_L * d_T * d_s} \qquad \textbf{Equation 1}$$

where d_L, d_T, and d_S were the mean grain sizes along the longitudinal, transverse and short transverse directions, respectively.

TEM study

Discs were cut by electro-discharge machining then profiled in a twin-jet polishing unit with 65% methanol, 32% butoxyethanol and 3% perchloric acid solution at 80 volts DC. The temperature was maintained at about -30°C. The TEM study was performed on a Philips 12 microscope using an accelerating voltage of 120kV.

Experimental results and discussion.

Grain growth and grain boundary pinning by second phase particles

Previous reports have shown that, in K-15 alloy, the grains grew rapidly with time when annealed at temperatures higher than 450°C after cold rolling with an 85% thickness reduction. It is known that large second phase particles promote fine grained microstructures during annealing after severe cold work[1]. Based on this effort, an aging treatment was carried out at 100°C and 150°C for three and four days, respectively, following homogenization of the as-received materials (Figure 9). The grain structures were only slightly refined in comparison with the material that was not aged (Figure 10). An initial grain size of about 5μm was obtained, but the grains grew continuously during static annealing at 500°C. The difference in grain growth rates between the aged and not aged materials was small. The grains grew more rapidly at 550°C for both alloys studied. Thus in spite of an intially fine grain size, microstructural stability did not exist.

The TEM study revealed that the concentration of second phase particles in both alloys was high. These particles were not uniformly distributed after the homogenization treatment, but the distribution became much more uniform after cold rolling and annealing. Figure 11 shows the microstructure of K-15 alloy that was examined after homogenization to identify the chemical composition of the particles.

Three types of particles were observed. The particles present in the boundaries were about 0.5μm and had irregular square shapes. They contained Al, Mg, Mn, Cr, and Cu. There were many long needle-shaped particles which contained Al, Cr, and Mn, occasionally with addition of Cu. The third group of particles had irregular shape and size, containing Al, Zr, and Cu. Some of these were found to contain Mg, while others had Mn. There was no strongly curved boundary being pinned by particles in this sample. The refined grain structures were not stable at the deformation temperatures in these alloy, perhaps because the particles present were larger than required to pin the boundaries. Further work is needed to compare alloys with different Cu content and with different pinning behaviors.

Superplastic flow and elongation

Tensile tests were conducted at 550°C and two constant strain rates, $4x10^{-3}s^{-1}$ and $4x10^{-4}s^{-1}$. The true stress-strain curves of the two alloys after various thermomechanical treatments are shown in Figure 12. Both alloys showed strain hardening at the strain rates used, especially at the faster rate. The cross-sectional area strains were measured near the fracture, and these data are also shown in the figure. The area strains were generally larger than those measured from the

gage length elongation. Alloy K-16 was generally softer than K-15 at both of the strain rates. Solution treated K-16, however, showed comparable flow stress with K-15 at the faster rate.

The strain rate sensitivity of the flow stress (*m* value) has been measured for the 5083-15 alloy at 550°C over a strain range. This is shown in Figure 13. The maximum value of about 0.6 was obtained at $2x10^{-3}s^{-1}$. The peak *m* value decreased and shifted to the lower strain rate range with increasing strain. Both strain hardening and the decrease of of *m* are believed to be primarily associated with strain-induced grain growth which is discussed in the next section.

The tensile elongation data, the grain size data obtained near the fracture surface of the specimens, and the volume percent of cavities are summarized in Table 4. Both K-15 and K-16 alloys showed large tensile elongation to failure, particularly at the low strain rate. The maximum elongation of about 939% was obtained from K-16 at $4x10^{-4}s^{-1}$. This specimen was aged at 150°C for four days before rolling, but was not solution treated before testing. A minimum elongation of about 223% was obtained from the same alloy with the same thermomechanical treatment, but at $4x10^{-3}s^{-1}$ strain rate. The K-15 alloy showed larger elongation at the low strain rate. The 200% tensile elongation is sufficient for forming most industrial parts if there is no cavitation damage.

The effects of aging and solution treatments on the superplastic response of the materials appear to be complicated. For the K-15 alloy, solution treatment before testing generally increased the material's elongation for both aged and non-aged conditions and at both strain rates. Aging before rolling generally decreased the elongation at both strain rates, although there was evidence that aging at 100°C for three days slightly increased elongation for the specimens which were not solution teated.

For the K-16 alloy at the low strain rate, aging with no subsequent solution treatment was generally beneficial for total elongation. At high strain rates, these effects were somewhat unclear.

In general, the effects of aging and solution treatments on both alloys were relatively small. A plot of total elongation versus strain rate is shown in Figure 14. Although the K-16 alloy showed good tensile elongation at $4x10^{-4}s^{-1}$, the elongation decreased rapidly when the strain rate was increased by an order of magnitude, despite the fact that the flow stress of K-16 was generally lower than that of K-15. At $4x10^{-3}s^{-1}$, the K-16 alloy exhibited elongations of 300% or less, while elongations greater than 400% were obtained from K-15. Since a faster deformation rate is beneficial in forming components, K-15 appears to be a better alloy.

The fast decrease in elongation with increasing strain rate in K-16 is not clearly understood at the present stage of investigation. There was evidence that the grain size of K-16 was larger than that of K-15. The strain rate sensitivity of K-15 was typically between 0.5~0.6 at 550C at the strain rates used. There is no such data for alloy K-16 yet. It is possible that alloy K-16 might have lower strain rate sensitivity at the fast strain rate. Further tests will be conducted to clarify this.

Several two-stage strain rate tests were conducted. In general, there was an improvement of tensile elongation when the alloys were first strained at a fast rate, normally $1x10^{-2}s^{-1}$, then continuously strained to failure at a slower rate, $1x10^{-4}s^{-1}$. The flow stress of the material after the first strain stage was generally lower than that if the material had been deformed only at the lower rate to the comparable strain. This behavior is believed to be due to a change in the grain structure. At higher strain rates, the material exhibited little dynamic grain growth. Therefore,

when the strain rate was decreased, the flow stress of the material was comparable to that if the material had only been deformed at the second rate.

Strain-induced grain growth and cavitation

Initially, the grains in both alloys were equiaxed but were elongated after deformation. A micrograph of K-15 alloy deformed to failure at 550°C and $4x10^{-3}s^{-1}$ is shown in Figure 15. Despite the differences in grain size in these alloys, the grain aspect ratio remained almost constant at about two, as seen in Table 4. The generally accepted observation that grains retain their equiaxed shape during superplastic deformation did not occur in these alloys. The significant grain growth during deformation may have resulted from the strain hardening and decrease of strain rate sensitivity.

A comparison of dynamic and static grain growth at different strain rates, obtained from the gage and corresponding grip sections of tested specimens, has been made at a common reference time (Figure 16). It appeared that the dynamic grain growth rate was faster.

Solution treatment before testing largely reduced the cavity volume for K-15 alloy, for both the aged and not-aged conditions and at both strain rates. Both the elongation data and the cavity volume indicate that solution treatment but no aging would result in better superplastic properties for K-15.

For the K-16 alloy, the solution treated specimens showed less cavities at the slow strain rate than the aged specimens. At the fast strain rate, the aged specimen without the solution treatment showed less cavitation damage after 337% elongation. Elongations were much less than with the K-15.

References

1 Humphreys, F.J., *Metal Science, 13* (1979) 136.

Table 4. Summary of tensile elongation, dynamic grain growth and cavitation.

K-15A, solution treated at 500°C for 0.5 hour before testing.

Strain rate (s^{-1})	aging before rolling	tensile elongation (%)	Area strain near fracture	Mean grain size (μm)	Grain aspect ratio	Average cavity volume (%)
$4x10^{-3}$	none	530	1.98	11.1	2	6.7
	100°C; 3 days	404	1.73	11.6	2.3	2.1
	50°C; 4 days	372	1.52	13.1	1.9	1.1
$4x10^{-4}$	none	853	2.6	19.8	2.1	2.6
	100°C; 3 days	837	2.64	16.8	1.8	4.2
	150°C; 4 days	735	2.57	20.1	2.2	1.7

K-16A, solution treated at 500°C for 0.5 hour before testing.

Strain rate (s^{-1})	aging before rolling	tensile elongation (%)	Area strain near fracture	Mean grain size (μm)	Grain aspect ratio	Average cavity volume (%)
$4x10^{-3}$	none	313	1.41	13.6	2.1	4.3
	150°C; 4 days	239	1.25	13.1	1.7	3.6
$4x10^{-4}$	none	680	2.25	19.5	1.9	5.1
	150°C; 4 days	750	2.43	21.4	2.1	7.7

K-15A, no solution treatment before testing.

Strain rate (s^{-1})	aging before rolling	tensile elongation (%)	Area strain near fracture	Mean grain size (μm)	Grain aspect ratio	Average cavity volume (%)
$4x10^{-3}$	none	435	2.05	12.2	2	10.2
	100°C; 3 days	522	2.06	12.8	2.1	12
	150°C; 4 days	463	1.99	12.5	2.3	10
$4x10^{-4}$	none	711	2.63	17.9	2.1	6.4
	100°C; 3 days	735	2.48	16.6	1.9	5.4
	150°C; 4 days	686	2.41	17.5	2.1	8

K-16A, no solution treatment before testing.

Strain rate (s^{-1})	aging before rolling	tensile elongation (%)	Area strain near fracture	Mean grain size (μm)	Grain aspect ratio	Average cavity volume (%)
$4x10^{-3}$	none	223	1.2	11.9	3	
	150°C; 4 days	337	1.52	13.7	2	1.3
$4x10^{-4}$	none	790	2.58	18.2	2.5	8.1
	150°C; 4 days	939	2.62	18	1.7	12.1

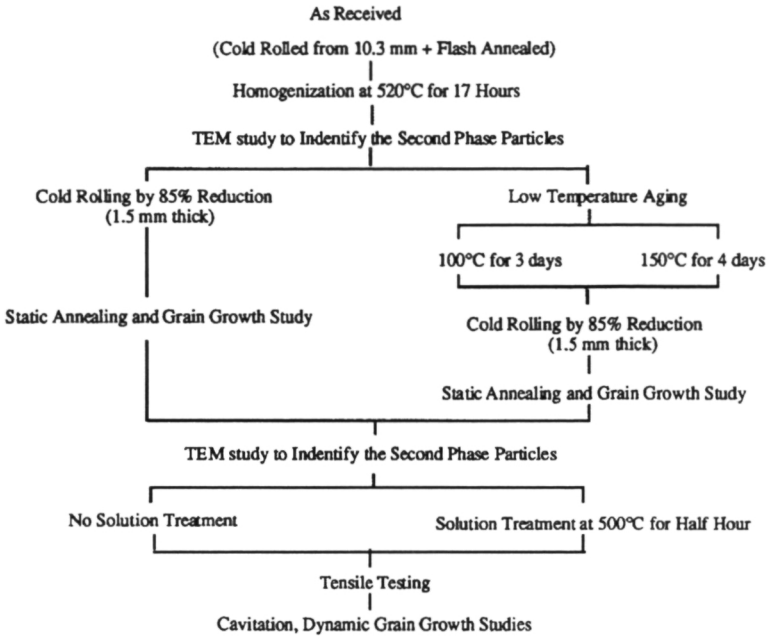

Figure 9. Thermomechanical processing and testing schedule for alloys K-15 and K-16.

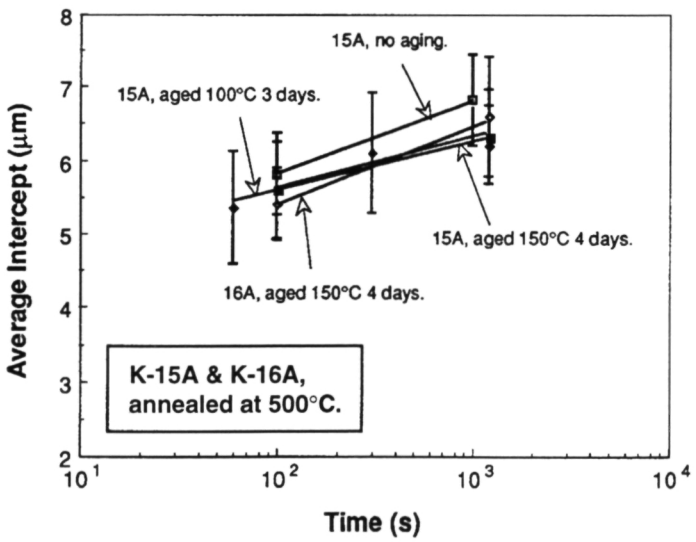

Figure 10. Static grain growth behavior of K-15 and K-16 alloy at 500°C aging treatment before rolling slightly refined the grain structure.

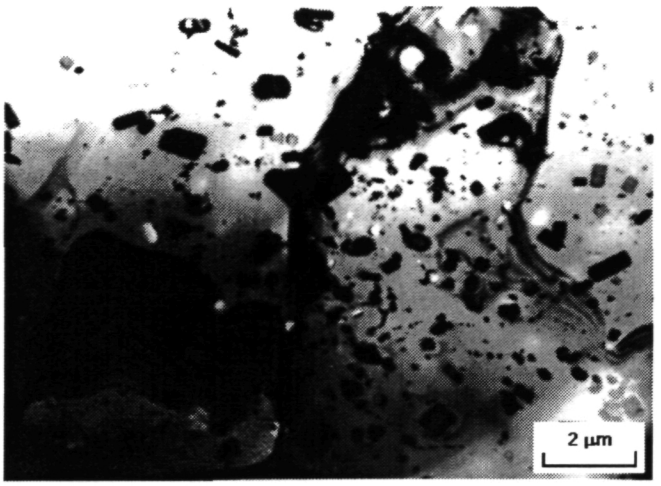

Figure 11. Multiple beam bright field TEM image of K-15A, showing the second phase particle configuration. The sample was cold rolled to an 85% thickness reduction, then annealed in a salt bath at 500°C for 0.5 hour and quenched in water.

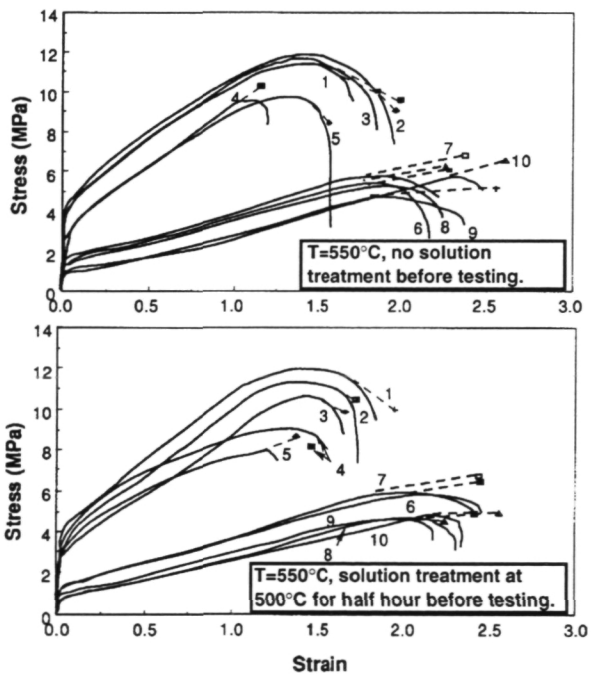

Figure 12. The flow behavior of K-15 and K-16 alloys after various thermo-mechanical treatments. The area strains which are generally larger than strains measured from elongation near fracture are also indicated in the figure.

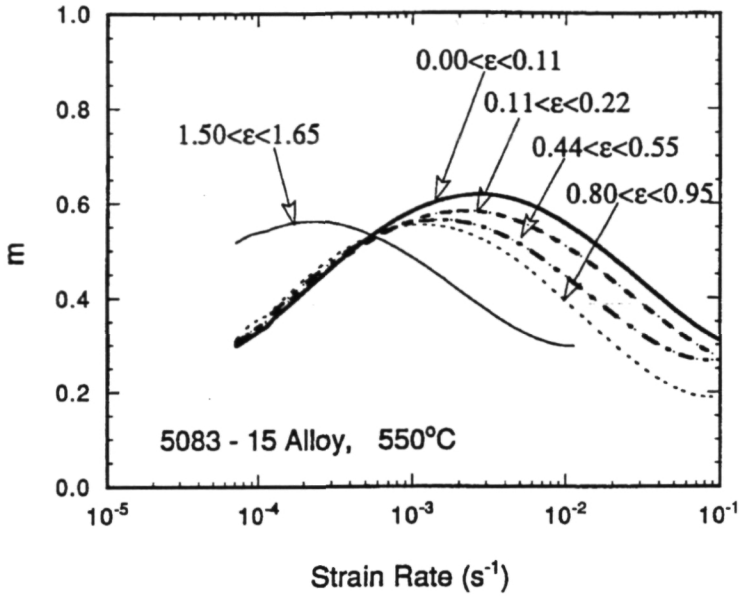

Figure 13. Strain rate sensitivity index as a function of strain rate measured from alloy K-15 at 550°C over a strain range.

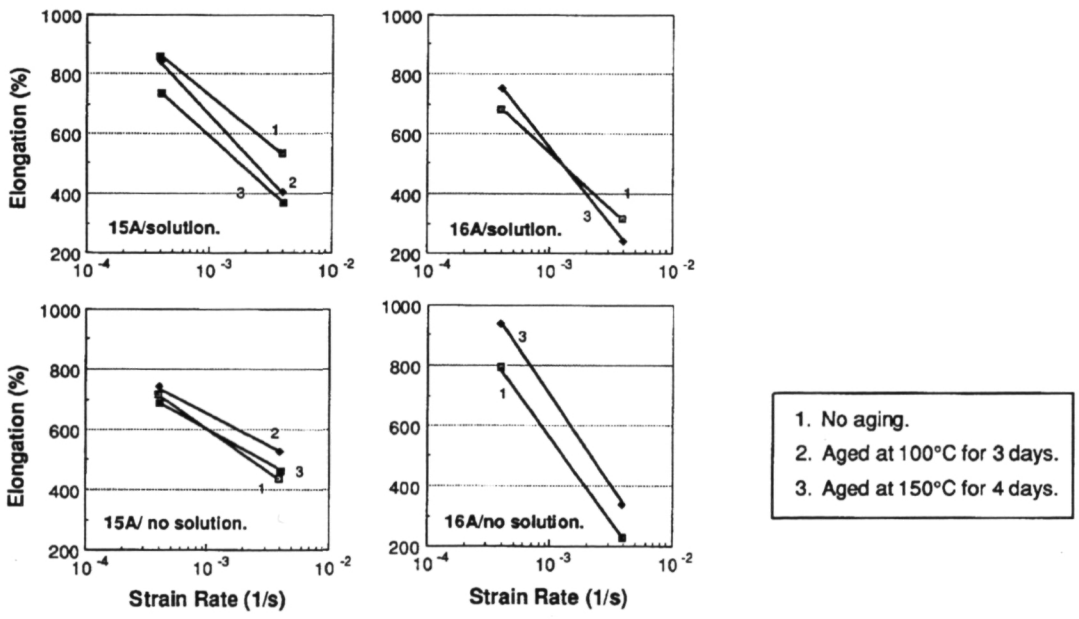

Figure 14. Total elongation versus strain rate for K-15 and K-16 alloys under various thermomechanical treatments. The elongation of K-16 descreases more sharply with increasing strain rate.

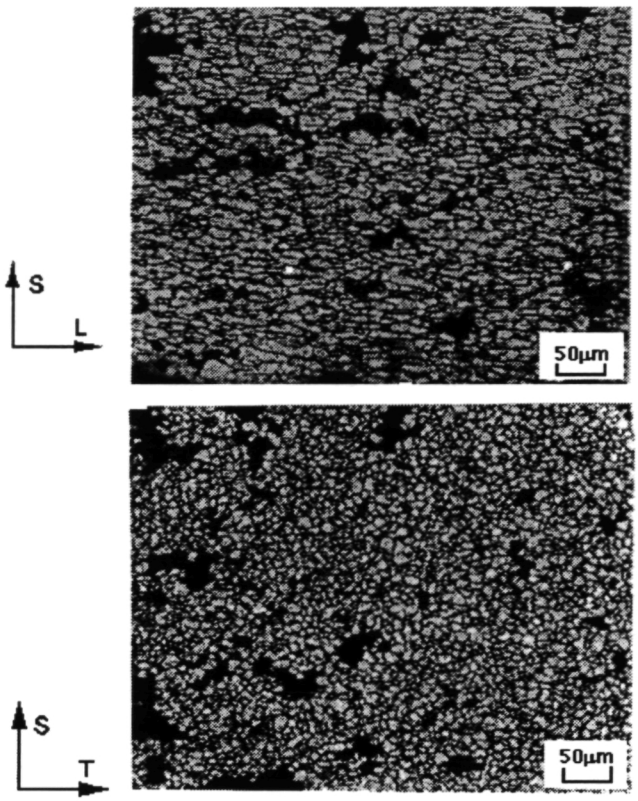

Figure 15. Optical micrograph showing cavity damage and grain structure of K-15 alloy tested at 550°C, $4x10^{-3}s^{-1}$. Grains were elongated in the tensile direction. Average gain size is about 12.2μm; grain aspect ratio is about 2.

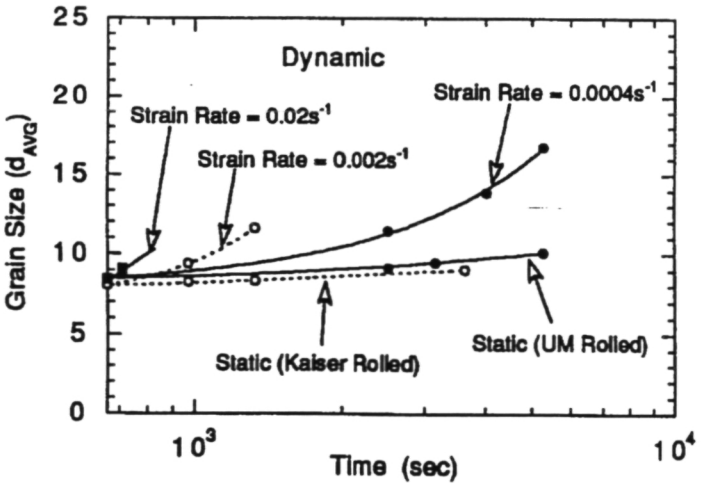

Figure 16. Dynamic and static grain growth at different strain rates determined at a common reference time.

Battelle Pacific Northwest Laboratories

1.1.3 Modify Composition of 5000 Al Alloys and Evaluate Structure Property Relationships

During this reporting period, alloys K-14, K-17 and K-19, containing various levels of Mn and Zr added to a base 5083 composition, were subjected to a series of thermomechanical treatments and evaluated by superplastic tensile testing. Detailed analysis of the microstructures of alloys 14, 17 and 19 were evaluated by optical metallography and scanning electron microscopy in the as-cast and as-rolled-and-annealed conditions to determine alloying constituent effects on particle size, morphology and distribution. As with the Cu/Zr modified 5083 alloys evaluated by GM R&D, the goal of this effort was to pare the alloy variants to a smaller number for final processing into a coil.

Thermomechanical Treatments

Earlier evaluations by PNL (see 4 month progress report) indicate that specimens preheated at 400°C for 24 hours and at 500°C for 10 hours were underaged and Mn remained in solution. In order to evaluate the effect of aging, and maximize the $Al_6(Mn,Cr)$ precipitate, a series of alloys were subjected to "reheat" treatments. Initially, a maximum practical aging time of 24 hours was established and aging temperatures of 500°C, 550°C, and 570°C were used. The resulting grain sizes for alloys 14 and 17 were not different for a given reheat condition. However, when these alloys were subjected to the reheat treatment, an increase in total extension over the baseline "A" process was observed in tensile testing at $1x10^{-3}s^{-1}$ at 500°C and 550°C. Figure 17 gives the total extension observed for alloys 14, 17 and 19 subjected to various "reheat" processes.

The effect of cold reduction on the superplasticity of alloys 14, 17, and 19 was evaluated by hot rolling the alloys to three initial thicknesses (6, 8 and 10mm) and cold rolling to a final gage of 2mm, to give cold reductions of 2:1, 4:1 and 5:1. Extension increased with cold reduction in all samples tested at $1x10^{-3}s^{-1}$ and 500°C and 550°C. The difference in extension between alloys processed using the "A" treatment and the 5:1 cold reduction was very slight, suggesting that cold rolling from 25mm to 10mm (impractical in a production environment) could be eliminated. Figure 18 shows the extension differences for alloys 14, 17 and 19 as a function of cold reduction.

Compositional Effects

The effect of alloying addition on the particles present in the alloys can be separated into two distinct categories: 1.) Dispersoids formed during precipitation reactions from the supersaturated solid solution developed during solidification; and 2.) Insoluble eutectic constituents formed during solidification.

Dispersoids

Zirconium was added to the 5083 compositions to develop a high volume fraction of Al_3Zr precipitates which, when processed properly, would stabilize a submicron substructure and recrystallize dynamically during straining at high temperatures in a process called continuous dynamic recrystallization (CDR). However, it was observed very early that recrystallization was not suppressed. Either a completely recrystallized or a super recovered structure was developed after short exposures to relatively low temperatures (250°C to 300°C). For low Mn content (0.8Mn), the "grain size" was actually larger for the Zr containing alloys. However, the Zr

addition delayed the onset of cavitation for the alloys even though the alloys had larger grain sizes and lower overall elongations. This is contrary to what might be expected from an addition which produces fine precipitates. It would be expected that the fine precipitates might actually promote cavitation if they resided on grain boundaries.

Manganese was increased in the modified alloys to produce more $Al_6(Mn,Cr)$ precipitates for many of the original reasons proposed for the Al_3Zr. The Al_6Mn appeared to be a more effective boundary pinning precipitate than the Al_3Zr due to the fact that grain size decreased with increasing Mn content. This was initially attributed to the size and distribution of the Al_6Mn, since it is present as large clusters, more homogenously distributed in the alloy than the banded Al_3Zr.

Eutectic Constituents (ECs)

The desire to produce a high forming rate CDR alloy has been the goal for developing alloys with high volume fractions of fine precipitates. However, a stabilized subgrain structure has not been attained at any temperature over 300°C utilizing practical processing. WSU observed some decrease in the rate at which recovery/recrystallization occurred but no actual suppression. There apparently is an overwhelming nucleation source available, such as the insoluble eutectic constituents formed during solidification in conventional 5083. In 5083 the eutectic constituent is the $Al_6(Mn, Fe, Si...)$ particle which is fractured and redistributed during the rolling reduction processes. The following observations have been made:

Zirconium has a dramatic effect on the morphology of the eutectic constituents (ECs) present in the as-cast and as-rolled structure. As shown in Figure 19, the EC particle morphology of alloys 14 and 19, which do not contain Zr, can best be described as "Chinese script" with short dimensions of 2μm and long dimensions of up to 40μm. In alloy 17, which contains Zr, the ECs are blocky, on of the order of 5μm in "diameter." The EC size in Zr-containing alloys is relatively independent of Mn content, however, the volume fraction is a function of Mn. Therefore the resulting interparticle spacing of the EC in low Mn alloys is greater, resulting a larger grain size. The chemistry of the ECs, as determined by electron diffraction spectroscopy (EDS), is the same for Zr and no-Zr alloys. In order to quantify the morphology differences in the EC particles, a form factor has been calculated for alloys 14 and 17 and has been plotted in Figure 20. This illustrates the round particles found in alloy 17 compared to the higher aspect ratio particles found in alloy 14. Form factor is the ratio of perimeter to crossectional area. A round particle has a factor of 1 and a needle would approach zero.

The ECs in alloys containing Zr do not fracture and re-distribute to the same extent as in non-Zr, "Chinese script" alloys, which fracture sooner in the rolling process (during hot rolling) and are much more uniformly distributed by deformation. This is illustrated by the as-rolled structures given in Figure 21, which compares the relative constituent morphology for alloys 14, 17 and 19. Notice the more homogeneous distribution of finer particles in alloys 14 and 19 when compared to 17. Conversely, the distribution of the ECs in Zr-containing alloy sheet is only slightly changed from the as-cast structure (Figure 22). The ECs in Zr-containing sheet appear to have fractured very late in the rolling process. This fact raises several important issues:

1. Consistent with the large primary particles, the fracture of the large blocky ECs undoubtedly contributes to cavitation.

2. The nucleation associated with the Zr-containing alloys must be less TMP dependent, and a less rigorous TMP may produce the same structure.

3. The Zr-containing alloys may be sensitive to casting conditions. There may be a critical cooling rate which controls size and distribution of the ECs. In addition, zirconium may actually improve the castability. These effects can be demonstrated conclusively only by a large scale casting.

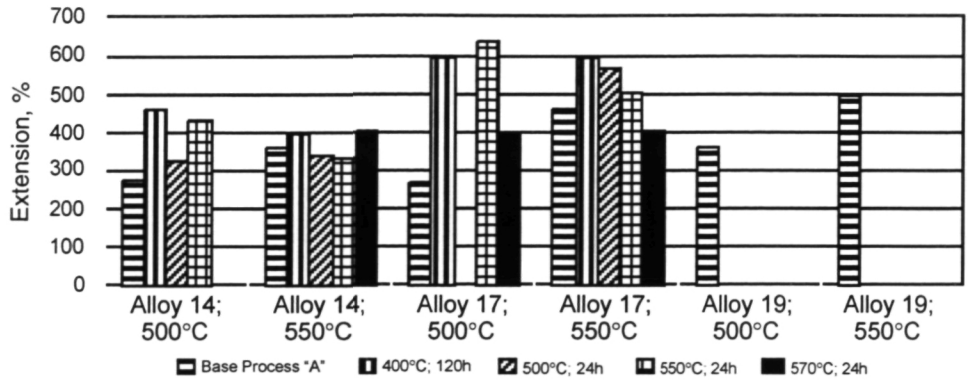

Figure 17. Effect of reheat (aging) on total extension for 5:1 cold reduction of alloys 14 and 17 and alloy 19A tested at $1x10^{-3}s^{-1}$ and 500°C and 550°C. Notice that with the additional aging step tensile properties in excess of alloy 19A have been achieved in alloys 14 and 17.

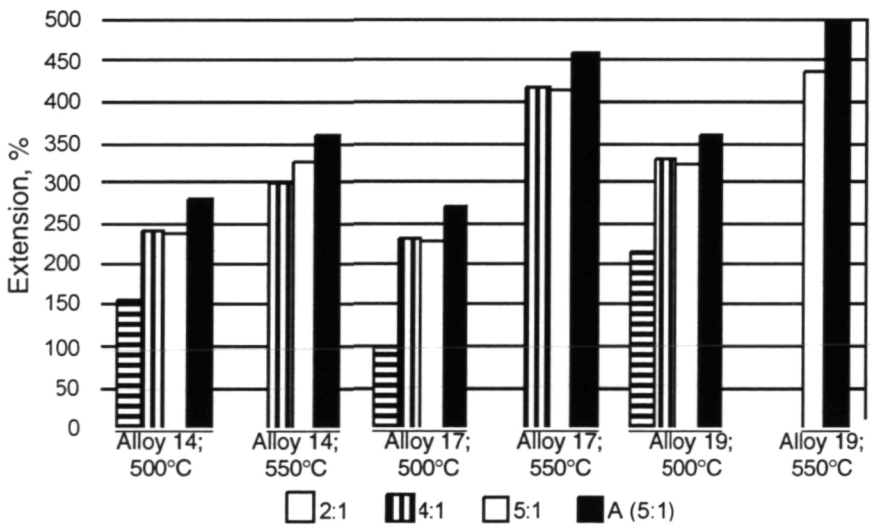

Figure 18. Effect of cold reduction on the tensile properties of alloys 14, 17 and 19 given cold reductions 2, 4, and 5:1 (tested at 500°C and 550°C, standard preheat, strain rate $1x10^{-3}s^{-1}$). Notice the relatively close values for the A process compared to the 5:1 cold reduction. This indicates the the impractical step of cold rolling from 25mm to 10mm may not be required to develop optimum properties.

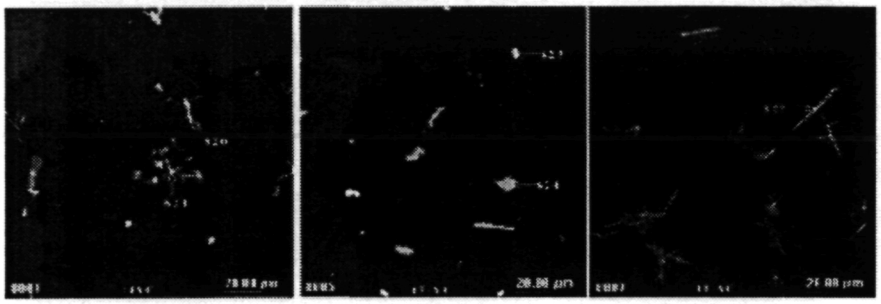

Alloy 14 Alloy 17 Alloy 19

Figure 19. As-cast shape of eutectic consituent particles, all with virtually the same composition.

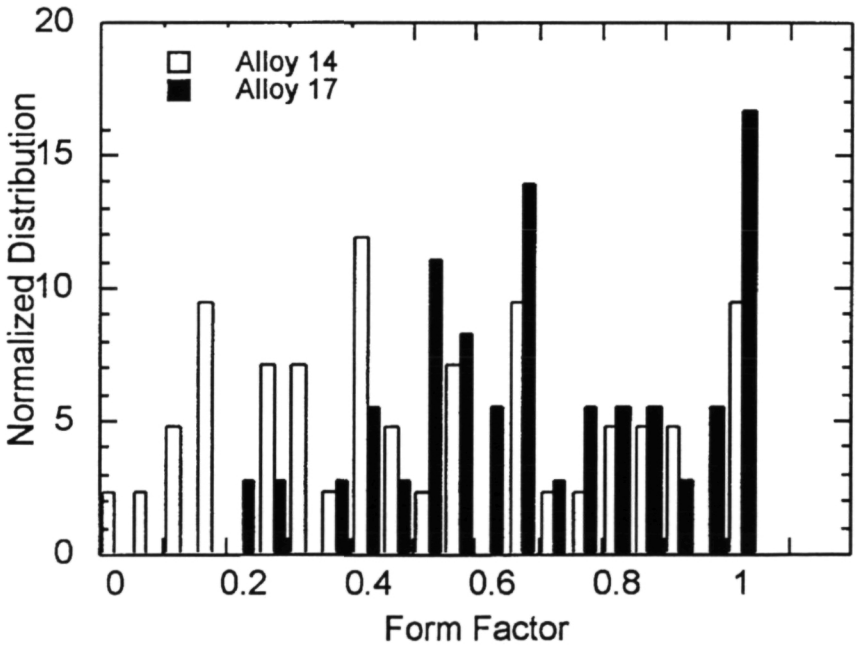

Figure 20. Form factor (needle shape = 0; round particle = 1) for eutectic constituents in alloys 14 and 17 as-cast.

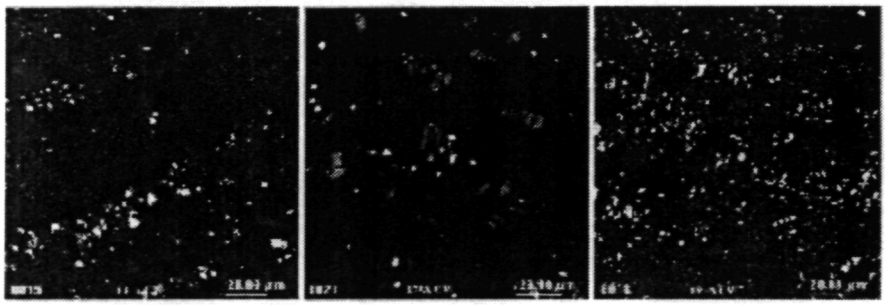

Alloy 14 Alloy 17 Alloy 19

Figure 21. As-rolled distribution of eutectic constituent particles.

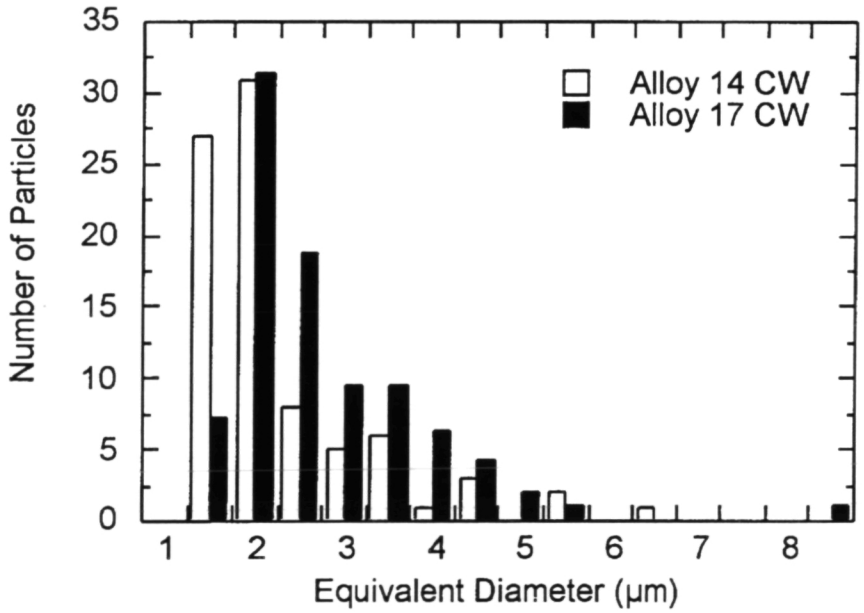

Figure 22. Distribution of broken eutectic constituents in alloys 14 and 17 following CW.

TOPIC 2–MANUFACTURING PROCESSES

STATEMENT OF WORK:

Effort in the nine-to-twelve month period of SPITFIRE-1 centered on evaluating post-SPF mechanical properties, including thickness measurement and tensile property determination, an assessment and selection of rapid forming approaches to pursue in the future, and pressure-time cycles for producing satisfactory test pieces. Significant progress was made on multi-sheet forming of aluminum.

2.1 AND 2.2 BASELINE MANUFACTURING PROCESSES AND RAPID FORMING ALTERNATIVES

General Motors Research and Development Center

This report documents the determination of the baseline manufacturing practices in commercial superplastic forming (SPF). Currently, GM is investigating possible hybrid SPF operations. The tooling required for exploratory experimentation in this area at GM is complete. Initial experiments should be completed by the start of fall. The properties of formed components are also being evaluated. Pans with thickness strains exceeding 60% have been formed and the post-formed mechanical properties will be determined.

As a conclusion to SPITFIRE-1, GM has established criteria for rapid SPF. For manufacturing, the maximum allowable cycle time for any part will be 10 minutes. However, for the component properties, more data needs to be generated before a criteria can be established.

2.1.1.13 Conduct exploratory tests on hybrid forming.

One method proposed by GM to reduce the SPF forming cycle is a hybrid conventional stamping/SPF operation. By conventionally drawing the sheet to a certain depth prior to SPF, the amount of superplastic strain required to form the final part would be reduced significantly. Therefore, the SPF strain rate could conceivably be higher in finishing the part. However, there are some questions that exist with this approach. First, the depth of draw one can expect out of an SPF alloy is unknown. Second, the plastic strain produced in the preformed sheet will most likely induce grain growth, destroying the superplastic properties of the sheet. Tests are underway to determine the amount of strain that can be produced in the preform and still retain a fine grain size.

Currently, GM R & D has a experimental draw die with a 33mm x 38mm cavity. An identical tool suitable for SPF has be constructed at GM. This way, a part can be partially preformed in a conventional stamping press and then placed in the SPF die and formed. Optimization of the pressure-time cycle for the hybrid SPF tool will begin in late summer. Hybrid forming trials will begin later; the stamping tool is currently being modified and will be installed in the press about mid-September.

2.1.2.3 Determine post-SPF mechanical properties

The 320-ton superplastic press by Superform U.S.A. that was purchased by GM is now operating. Superform also constructed a 533mm x 610mm pan die for General Motors with back pressure capability, and is currently being used to form parts. Since this pan is very deep (190mm), the maximum thickness strain can exceed 60%. Pans have been formed at various strain rates and will be sectioned for the destructive evaluation of mechanical properties. The post-formed tensile properties and the volume fraction of cavitation will be measured as a function of strain and strain rate.

2.1.3.2 Establish processing targets for rapid SPF

After evaluating the current state of practice in SPF, it was determined that the current forming cycle is too long for high volume production. For SPF to be feasible in automotive production, the forming cycle should last no more than 10 minutes for any part. However, as in any high production operation, a faster forming cycle will always be more favorable.

2.1.3.3 Establish post-SPF property targets for rapid SPF

Currently, GM needs to gather more data on the post-SPF properties of manufactured components before it can establish the post-SPF property targets. Work is currently underway to evaluate stress corrosion cracking, post SPF mechanical properties and post-SPF dimensional tolerance. After these tests are complete, a more accurate evaluation of the post-SPF properties can occur.

2.1.1 - ESTABLISH FORMING PARAMETERS FOR EXISTING MANUFACTURING PROCESSES FOR SUPERPLASTIC ALUMINUM AND 2.1.2 - EVALUATE THE QUALITY OF MANUFACTURED COMPONENTS

Pacific Northwest Laboratory

The current reporting period represents ten months of effort (instead of the scheduled twelve), and the majority of the sub-tasks under Task 2.1.1 have been accomplished. For Task 2.1.2, studies of cavitation as a function of strain and strain rate (sub-task 2.1.2.2) have been largely completed for uniaxial tensile specimens and Alloy 19 formed trays. Additional cavitation studies, as well as evaluation of backpressure forming, were completed by mid-July.

Forming experiments using Alloy 19, a modified 5083 alloy, were completed during this reporting period, to verify modeling predictions for the associated DOE-ER project. Data generated from these experiments were used to evaluate the effects of strain and strain rate on cavitation and thickness distribution. A comprehensive forming test matrix utilizing Alloy 12 and 13 sheet has been formulated and will be performed during the next reporting period. This study will demonstrate forming at three strain rates and will determine the optimum constant strain rate range for Alloy 12 based on thickness distribution and cavitation levels.

Experimental Forming of Alloy 19

The primary focus of the Alloy 19 forming experiments were to verify modeling and simulation predictions in support of the associated DOE ER-LTT CRADA effort. Results of this work are reported in a separate letter report, *Experimental and Modeling Results for Modified*

5083 Al (Alloy 19). The Alloy 19 forming work included examination of sheet thickness distribution and cavitation as a function of strain rate. Results of these destructive evaluations are included in the section of this report covering Task 2.1.2.

Forming cycles conducted on Alloy 19 show the potential for rapid forming of components using conventional constant strain rate pressure/time histories. Tray forming experiments were performed at rates of $1 \times 10^{-3} s^{-1}$, $5 \times 10^{-3} s^{-1}$, $7.5 \times 10^{-3} s^{-1}$, and a rate estimated to be greater than $1 \times 10^{-2} s^{-1}$. Resulting tray forming times were 14 min., 2 min. 30 sec., 1 min. 40 sec., and 26 sec., respectively. Tray number 65B, which was run at a rate greater than $1 \times 10^{-2} s^{-1}$, displayed a higher level of thinning over the die entry radius. The three trays run at the lower constant strain rates displayed relatively good thickness distribution. A listing of the Alloy 19 tray forming experiments is included in Table 5. Significant results of this work that benefit the SPITFIRE program are: 1) demonstration of accurate modeling methods for generation of pressure/time histories for constant strain-rate forming, 2) demonstration of rapid forming cycles (100 sec. for a complete tray) using conventional gas pressure forming (i.e., without the use of variable strain path approaches), and 3) rapid forming capability of a modified A1-5083 alloy.

A limited effort was also conducted to evaluate the effect of low forming temperature on tray quality and formability. Sheets of Alloys 19, 12, and 13 were formed at 500°C using a constant strain rate of $5x10^{-3} s^{-1}$. A comparison of the pressure/time history required for the $5x10^{-3} s^{-1}$ strain rate is shown in Figure 23, and as indicated, forming of Alloy 19 at the lower temperature requires significantly higher gas pressure throughout the forming cycle. Although relatively comparable forming times were achieved at 500°C, thickness measurements indicate more pronounced thinning in the die entry radius for Alloys 19 and 12. Comparison of the die entry radius area for Alloy 19 tray 58B ($5x10^{-3} s^{-1}$/550°C) and tray 68B ($5 \times 10^{-3} s^{-1}$/500°C) shows a minimum thickness of 0.12mm and 0.10mm for the 550°C and 500°C forming temperatures, respectively. The Alloy 13 tray ruptured during the early stages of forming.

Completion of Task 2.1.1 includes the optimization of forming cycles (sub-task 2.1.1.7) and evaluation of the effect of backpressure (2.1.1.9) on part forming and part quality (2.1.2.1). A comprehensive test matrix has been developed based on forming of Alloy 12 sheet, which is available in greater quantity than Alloy 19. Objectives of the experiments include evaluation of forming behavior in the longitudinal (length in the rolling direction) and transverse sheet orientations, effect of backpressure on sheet forming, and comparison of forming behavior at two different temperatures (550°C and 500°C).

The focus of Task 2.1.2 is to evaluate the effect of forming on part quality. The first part of this task was completed with the evaluation of Alloy 19 tray thickness and cavitation behavior at four strain rates. The thickness profiles for the three partially formed trays, including the die flange, die entry radius and center sections are plotted in Figure 24. As the results indicate, the higher strain rate (63B, $7.5x10^{-3} s^{-1}$) resulted in greater thinning in the die flange area (more material pulled into the tray portion), and less thinning in the die entry radius. The net result is that tray formed at the higher rate ($7.5x10^{-3} s^{-1}$) actually displays a more uniform thickness distribution than the trays formed at the lower rates (53B and 56B). An attempt was made to form a tray to completion using a pressure ramp of 3.4 MPa in one minute, with the ramp being run for 26 seconds. Although the tray (65B) was nearly complete in less than 30 seconds, more thinning was observed in the die entry radius (0.93mm) when compared with the lower forming

rate trays. Reverse modeling of the pressure/time history indicates that the strain rate for this tray exceeded $1x10^{-2}$ s^{-1}, with localized areas (die entry radius) reaching $3.9x10^{-2}s^{-1}$. These results appear to indicate that the forming rates generated for tray 65B exceed the optimum rate for Alloy 19.

Cavitation was evaluated in the fully formed trays using samples sectioned from the plane-strain portion of the tray (mid point of the tray length), and Figure 25 shows the results for the Alloy 19 trays formed at the four different strain rates. The general trend observed for the trays is increasing levels of cavitation with increased strain rate, with the exception of tray 61B, which shows less cavitation than tray 58B, which was formed at the slower $1x10^{-3}s^{-1}$ rate. Tray 65B shows somewhat greater cavitation throughout the sample, with a higher concentration of cavities in the die entry radius region where the localized thinning has occurred.

Figure 26 provides a similar series of micrographs for the three trays formed at the lower 500°C temperature. The figure illustrates several important features of the different alloys. A general observation is that Alloy 19 cavitation occurs in stringers associated with primary intermetallic particles, while Alloy 12 displays more uniform, evenly distributed cavitation. The Alloy 13 sample, which did not fully form, shows a very high concentration of large cavities concentrated in the area of failure. Away from the die entry radius, very little cavitation is observed, which is probably due to the combination of low elongation and strain rate that the material saw prior to rupture. Although a tray was successfully formed with Alloy 12 at 500°C using a relatively high strain rate, examination of the thinned area associated with the die entry radius shows a concentration of cavities. Additional cavitation studies are planned on the Alloy 12 and 13 trays that will be formed during the Task 2.1.1 effort. This will provide a more complete evaluation of the effects of temperature (500°C vs. 550°C) and strain rate. In addition, trays formed with and without back pressure will be evaluated.

Table 5. Test matrix for Alloy 19 tray forming.

Tray	Program	Strain rate (s^{-1})	Forming time	Comments
Sheet 1	53B	1×10^{-3}	6 min.	Tray depth > 1.0 ≈ 9.5mm flat, tray was sectioned, thickness available
Sheet 2	54B	1×10^{-3}	3 min.	Tray depth 17.5mm
	59B	5×10^{-3}	3 min. 22 sec.	Tray formed with 4mm side radius, tray was sectioned, thickness is available
Sheet 3	55B	5×10^{-3}	1 min. 12 sec.	Tray depth > 1.00 ≈ 6.35mm flat, tray was sectioned, thickness available
Sheet 4	56B	5×10^{-3}	1 min. 12 sec.	Tray depth > 1.00 ≈ 6.35mm flat
	60B	5×10^{-3}	3 min. 22 sec.	Tray formed with < 3mm radius prior to blow out. Tray ruptured at 3 minutes (pressure = 2 MPa).
Sheet 5	57B*	?	25 sec.	Cycle was aborted.
	57B	1×10^{-3}	14 min.	Tray formed ≈ 4.4mm edge radius, tray was sectioned, thickness is available
Sheet 6	58B	1×10^{-3}	14 min.	Tray formed ≈ 4.4mm edge radius, tray was sectioned, thickness is available
Sheet 7	6lB	5×10^{-3}	3 min. 22 sec.	Tray formed ≈ 4.4mm side radius
Sheet 8	62B	5×10^{-3}	2 min. 30 sec.	Tray formed ≈ 4.8mm side radius
Sheet 9	63B	7.5×10^{-3}	46 sec.	Tray depth > 1.0 ≈ 4.8mm flat
Sheet 10	66B	7.5×10^{-3}	100 sec.	Tray formed with ≥ 4.8mm radius
Sheet 11	65B	$> 1 \times 10^{-3}$	26 sec.	Tray formed with side radius 4.8mm, tray has extreme thinning in top radius.

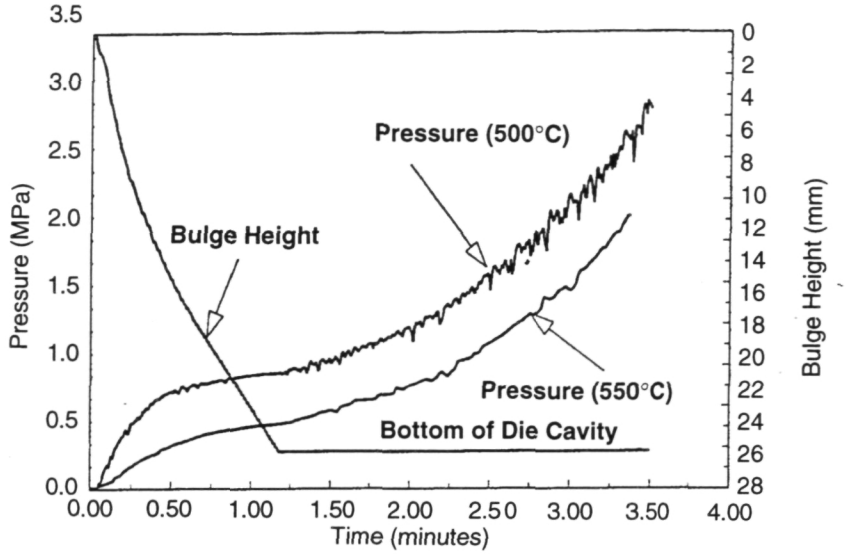

Figure 23. Pressure history and bulge height based on forming at two different temperatures, 500°C and 550°C.

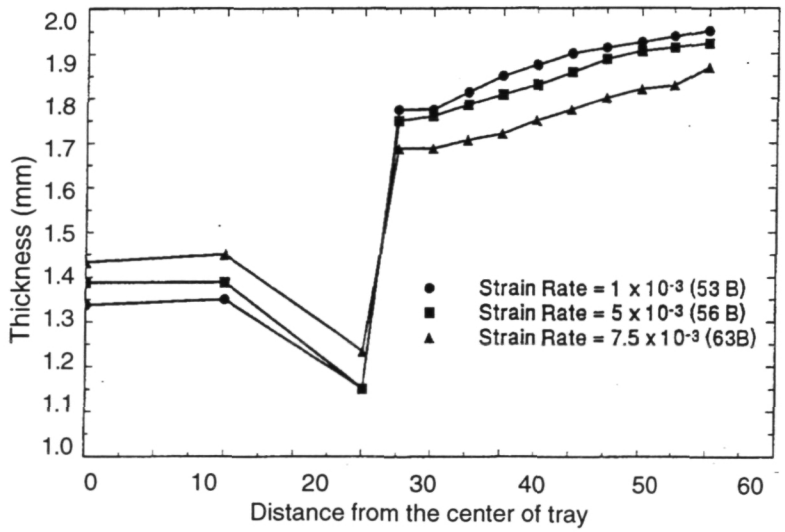

Figure 24. Thickness profile for alloy 19 trays (forming temperature = 550°C).

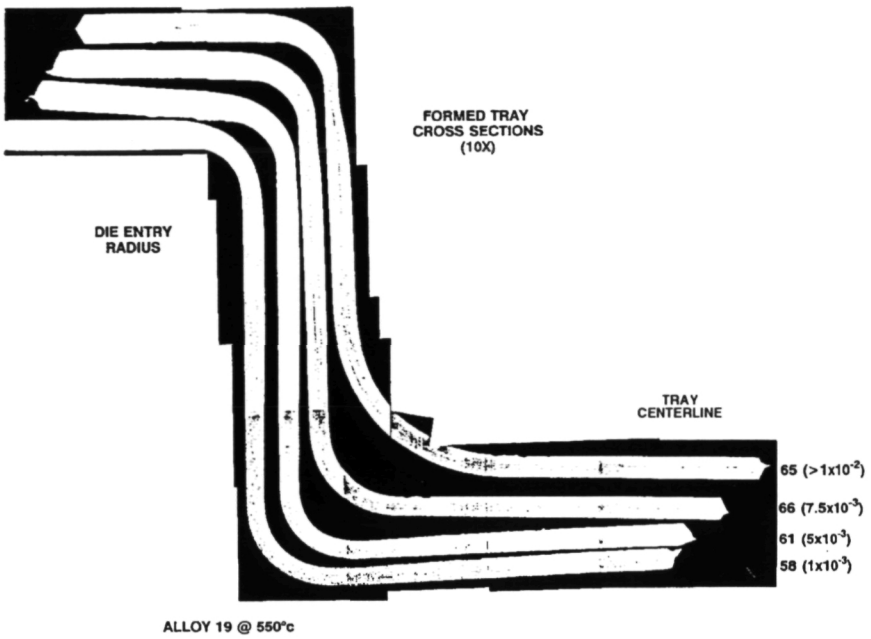

Figure 25. Formed tray cross sections (Alloy 19 @ 550°C).

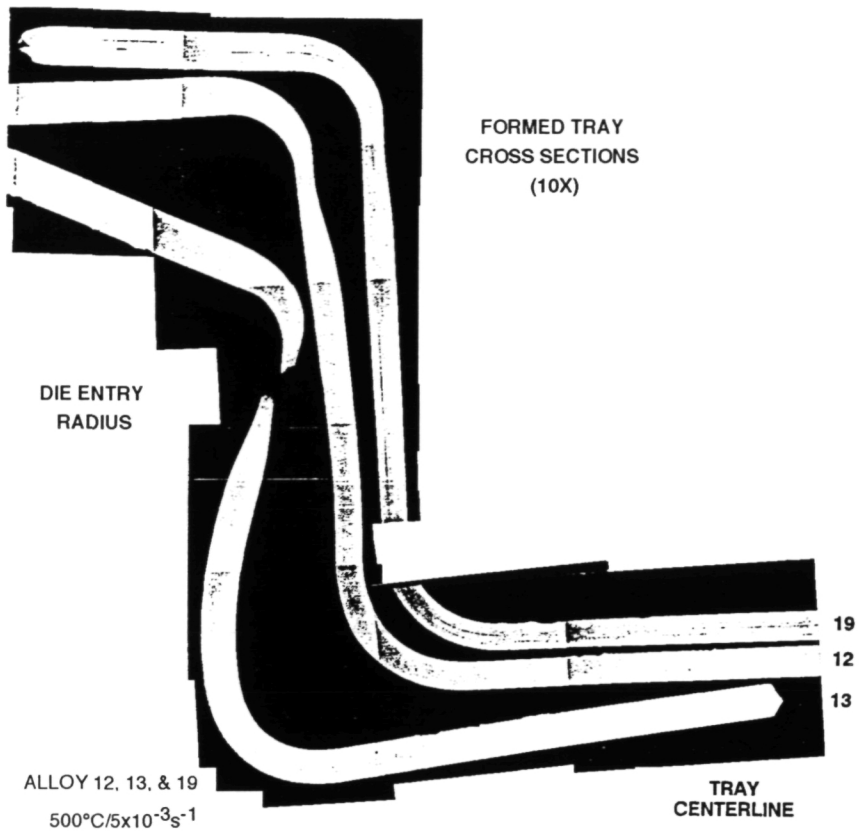

Figure 26. Formed tray cross sections.

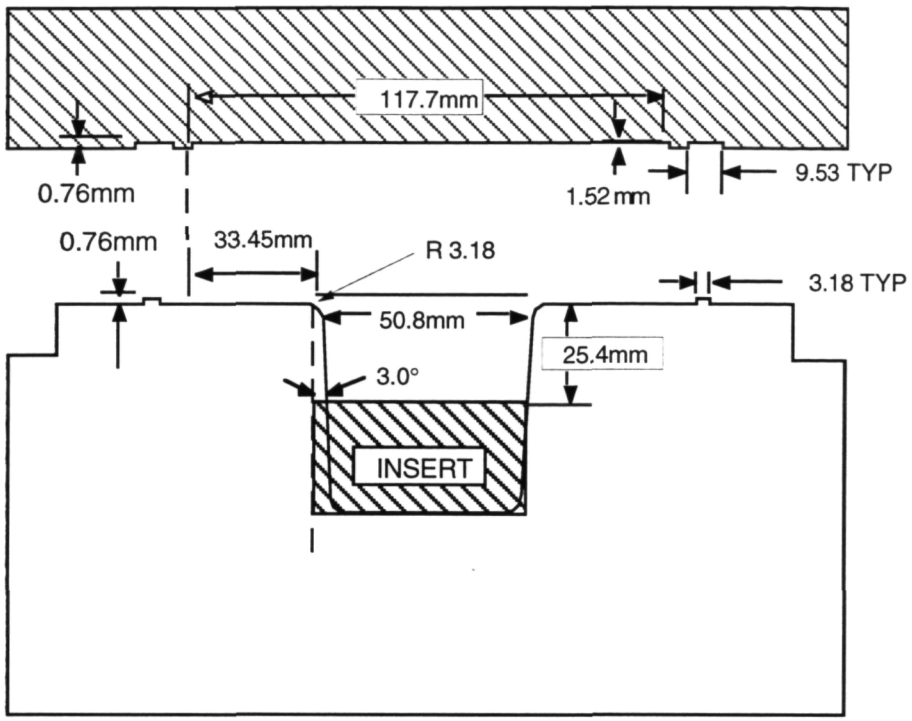

Figure 27. SPF butter tray die.

2.1.1-ESTABLISH FORMING PARAMETERS FOR EXISTING MANUFACTURING PROCESSES FOR SPF ALUMINUM AND 2.2.1-EXPLORE NEW CONCEPTS FOR MAKING SPF ALUMINUM COMPONENTS AT A FASTER RATE.

NASA Langley Research Center

The following section summarizes progress at NASA LaRC on Tasks 2.1.1.6-10, 2.2.1.1, 2.2.1.2.

Rapid Biaxial Forming

In the last reporting period, 2 mm thick sheets of SKY 5083 were biaxially formed at 525°C into panels with the beaded web configuration. [Note: The sheet thickness was previously misstated in the 9-month progress report as 2.5 mm.] The pressurization cycle, shown in Figure 28, was designed to maintain a constant strain rate of $1x10^{-3}s^{-1}$ to bottom contact (Stage I) followed by $5x10^{-4}s^{-1}$ to corner contact (Stage II). The region of maximum forming strain, ε_{max}, is located at the intersection of the web with the flange. Based on ε_{max}=1.2, the 32 minute cycle time corresponded to a nominal true strain rate ($\dot{\varepsilon}_{nom}$) of $6.3x10^{-4}s^{-1}$. Earlier uniaxial parametric evaluations of the material revealed that this is close to the optimum strain rate for superplastic forming.

In this reporting period, the primary focus was to reduce the cycle time for biaxial forming SKY 5083. A series of forming trials involving progressively shorter cycle times were conducted at 525°C. Based on uniaxial test results, forming at a faster, 'non-optimum' strain rate decreases the formability of the material. Therefore, the goal was to establish the maximum speed a complete panel could be formed without perforating the deforming sheet. As before, both back pressure and boron nitride solid lubricant were employed and all panels were subjected to a five minute preheat. Towards the end of the preheating stage, the regions on either side of the sheet diaphragm were pressurized to 3.5 MPa. The necessary forming stress was generated by creating a pressure differential across the sheet. During the forming cycle, the upper pressure was maintained at 3.5 MPa while the lower pressure was reduced. In contrast to previous trials, the pressure-time profile was not designed to approximate a constant strain rate.

The results of the forming trials are shown in Table 6. The baseline panel, 2/28/95B, was formed under optimum deformation conditions, i.e., 525°C and a two stage constant strain rate with a nominal strain rate of $6.3x10^{-4}s^{-1}$. The remaining panels, 4/13/95A - 4/14/95F, were formed at 525°C using non-optimum strain rates. All of the forming trials on SKY 5083 resulted in a complete pressurization cycle without sheet perforation. Due to the trial-and-error approach, a complete pressurization cycle did not necessarily culminate in complete panel formation.

The degree of panel formation was assessed by measuring the panel radius of curvature, r_{min}, and thickness, t_{min}, at the location of ε_{max}, i.e., the web-flange corners. Figure 29 shows a schematic of the beaded web panel cross section. Based on previous measurements from beaded web panels produced using prolonged post-forming dwell times at the maximum 3.5 MPa pressure differential, the criteria for complete panel formation were established as r_{min}=0.51 mm and t_{min}=0.61 mm. Panels 2/28/95B, 4/13/95A, and 4/13/95F have a web/corner $r_{min} \approx 1t_{min}$ and

show complete part formation. The faster non-optimum forming rate panels (4/14/95G and 4/14/95F) have $r_{min} \approx 2t_{min}$ to $3.5t_{min}$ and are not as fully formed.

The cycle times quoted represent the actual time that a pressure differential was applied to the sheet. Addition of the five minute preheating time provides the total forming time. Use of t_{min} and cycle time enable the calculation of ε_{max} and $\dot{\varepsilon}_{nom}$ for each panel. The results of the non-optimum forming rate trials reveal that the cycle time can be reduced by an order of magnitude compared to the baseline optimum strain rate. The $\dot{\varepsilon}_{nom}$ corresponding to the shortest cycle time (part 4/14/95F) meets the SPITFIRE goal for fast forming ($\dot{\varepsilon}=10^{-2}s^{-1}$).

In the next reporting period, the influence of temperature on the formability and cycle time of SKY 5083 material will be evaluated.

Part Quality

The next phase of the work effort assessed the effects of rapid forming on part quality. It was recognized that, as the cycle time decreases, the divergence from the optimum strain rate increases. Non-optimum forming conditions were expected to have a deleterious effect on thickness gradients and cavitation behavior in the SKY 5083 material. Thus, the ends of the beaded web panels were sectioned to measure thickness variations and determine levels of cavitation. Thickness measurements were made from the centerline of the cap to the centerline of the flange at increments of 2.5 mm. Figure 30 shows the thickness profiles and corresponding true thickness strains for the panels produced using the non-optimum pressurization cycles. The data show that the thickness gradient is relatively insensitive to $\dot{\varepsilon}_{nom}$ when sheet/die lubrication and back pressure are used.

Microscopic quantitative image analysis was used to measure the areal fraction cavitation in the various SKY 5083 panels. Metallographic mounts were prepared of the specimen cross-sections. Quantitative image analysis was conducted at five locations on the beaded web panels: cap centerline, cap/web corner, web mid-plane, web/flange corner, and flange centerline. Six to eight measurements were made at each location at 200X magnification. Secondary phase particles were digitally removed from the image and the areal fraction cavitation and number of cavities were calculated at each position. The results, summarized in Table 7, reveal that the areal fraction of cavitation was low; averaging less than 0.5% in all but the regions corresponding to ε_{max} (web-flange intersection).

During the next reporting period, assessment of the effects of fast forming on part quality will continue. The influence of back pressure and various die lubricants on formability, thickness gradients and cavitation behavior will be included. The test matrix is shown in Table 8 for panels which have already been fabricated. Preliminary indications are that only those panels which were formed using back pressure and lubrication in combination did not perforate. The level of cavitation present in the panels produced using non-optimum forming rates will be compared with those formed using optimum forming conditions.

Microstructural Characterization

Microstructural characterization of SKY 5083 included optical metallography and nominal grain size determination. Mean linear intercept (mli) methodology, in conformance with ASTM-E112, was applied to cross-polarized light images of anodized metallographic sections. Figure 31a and b show tri-planar optical micrographs of SKY 5083 (panel 2/28/95B) following

biaxial forming at 525°C and $\dot{\varepsilon}_{nom}$ of $6.3x10^{-4}s^{-1}$. Figure 31a shows the microstructure of the material from outside the gasket seal region which was heat cycled only and not subjected to any deformation (ε=0). Figure 31b illustrates the microstructure of the material from the web/flange corner, the most highly strained region of the panel (ε_{max}=1.2). Compared to the material that was only heat cycled, the SKY 5083 material undergoes some microstructural coarsening during deformation. Although the deformed material has a slightly larger grain size, the grain morphology appears relatively unaffected.

The changes in grain size and grain shape for SKY 5083 are summarized in Table 9. Measurements were performed relative to the three principal axes (L, T and S) in the SKY 5083 material in the as-received condition and following deformation at 525°C and $\dot{\varepsilon}_{nom}$ of $6.3x10^{-4}s^{-1}$. The true strains represent different sections from the beaded web panel. As mentioned, the ε=0 area represents material from outside the gasket seal that was heat cycled only. The ε=0.1 area represents material from the centerline of the cap; ε=0.65 from the mid-section of the beaded web; and ε=1.16 from the web-flange corner.

In terms of grain coarsening, heat cycling alone equates to a total time at temperature (525°C) of 37 minutes. Static annealing of the as-received, fully recrystallized material results in a small increase in the nominal grain diameter and retention of the elongated grain morphology. The material exhibited somewhat more grain coarsening during deformation processing, ranging from d_{nom}=13 μm in the ε=0 region to d_{nom}=17 μm in the ε=1.16 region. In terms of grain morphology, the in-plane L/T ratio remains constant, but the through-thickness L/S ratio increases during deformation processing. The grains are apparently becoming more elongated parallel to the L direction, which is also the prior rolling direction in the as-received sheet.

In contrast to conventional wisdom, the grain morphology does not become progressively more equiaxed with increasing strain. Overall, the results indicate that the microstructure is relatively stable during deformation under optimum conditions. In the next reporting period, the multiple cone testing die will be used to monitor microstructure, texture development and cavitation behavior as a function of strain, strain rate and temperature for automotive and aerospace alloys.

Non-optimum forming trials were also conducted on other automotive and aerospace aluminum sheet materials included in the program. In all cases, the forming temperature employed corresponded to a homologous temperature, T_{SPF}/T_{MP} ~ 0.9. Complete panel formation was not achieved at any forming rate attempted on the conventionally processed automotive alloys; 5182, 6111 and 2008. Although the sheet ruptured prematurely, the 6111-T4 material showed the most promise and warrants further evaluation. In terms of aerospace alloys processed for superplasticity, rapid forming was successfully implemented for 8090, 2090, X2095 and Weldalite™ 049. Optimum and non-optimum forming trials continue with several superplastic versions of alloy 7475 supplied by different vendors.

Table 6. Results of Upper Limit Forming Evaluation.

Part Number	Time+	Web/Flange			$\dot{\varepsilon}_{nom}$ (s^{-1})
		r_{min} (mm)	t_{min} (mm)	ε_{max}	
2/28/95B*	32 min	0.51	0.61	1.20	$6.3x10^{-4}$
4/13/95A	27 min	0.53	0.61	1.20	$7.4x10^{-4}$
4/13/95F	6 min	0.71	0.66	1.12	$3.1x10^{-3}$
4/14/95G	2 min	1.60	0.71	1. 05	$8.8x10^{-3}$
4/14/95F	1.25 min	2.77	0.79	0.95	$1.3x10^{-2}$

* "Constant Strain Rate" pressurization cycle + Additional 5 min. heat-up

Table 7. Volume Percent Cavitation vs. Forming Rate.

Forming Time*	Cap_{CL} $\varepsilon \approx 0.1$	Cap/Web $\varepsilon \approx 0.3$	Web_{CL} $\varepsilon \approx 0.5$	$Flange_{CL}$ $\varepsilon \approx 0.5$	Web/Flange $\varepsilon \approx 1.2$
27 min	0.10	0.45	0.55	0.48	0.40
6 min	0.06	0.10	0.30	0.36	1.12
2 min	0.08	0.32	0.14	0.12	3.38
1.25 min	0.00	0.18	0.13	0.28	1.16

* "Non-optimized Strain Rate" pressurization cycles; additional 5 min heat-up

Table 8. Effect of back pressure and lubrication on the formability of SKY 5083 at 525°C.

Forming Cycle	Back Pressure	Lubrication		
		None	Boron Nitride	Graphite
Constant $\dot{\varepsilon}$	Yes	2/28/95B*	4/12/95C	—
Non-optimized $\dot{\varepsilon}$	Yes	5/4/95B*	5/4/95D	5/4/95D
	No	5/4/95A*	5/4/95C*	5/4/95E*

* Complete part formation, but sheet perforated

Table 9. Effect of SPF on the grain size of SKY 5083 (T_{SPF} = 525°C; $\dot{\varepsilon}_{nom} = 6.3x10^{-4}s^{-1}$)

True Strain	ASTM G#	d_{nom} (μm)	Aspect Ratios		
			L/T	L/S	S/T
As Rec'd	10.3	10	0.94	1.53	0.61
0	9.7	13	0.93	1.29	0.72
0.10	9.4	14	1.06	1.59	0.66
0.65	9.2	15	1.00	1.56	0.64
1.16	8.8	17	1.03	1.77	0.58

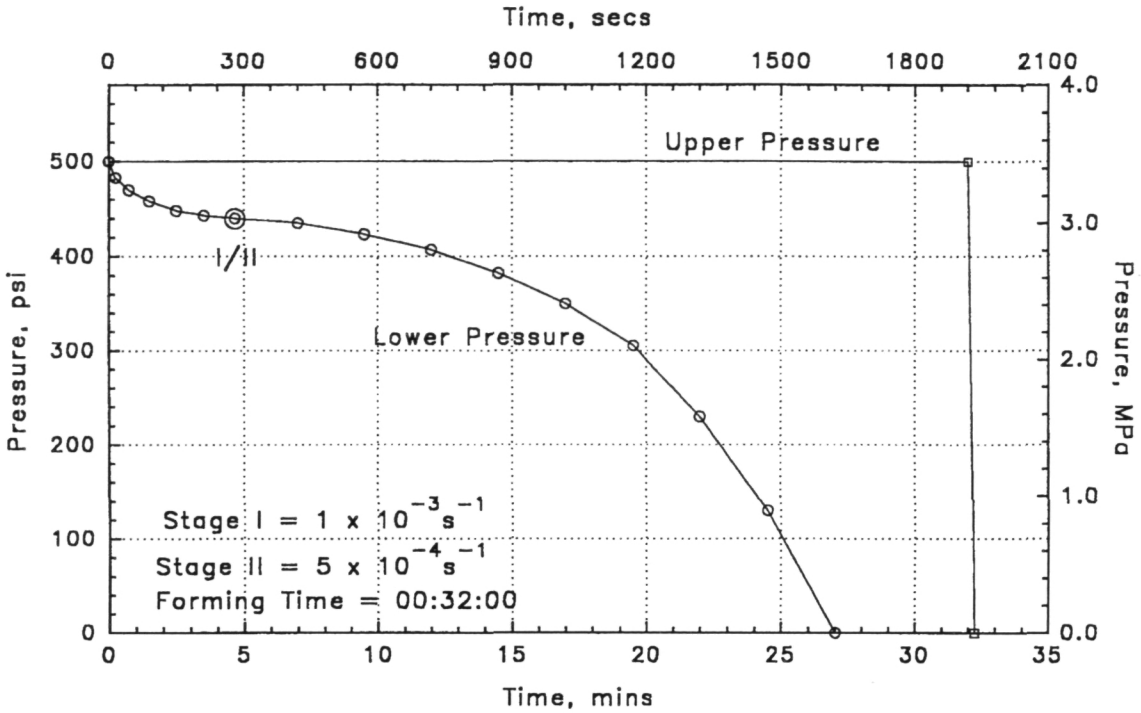

Figure 28. Pressure-time cycle for biaxial forming of SKY 5083 at 525°C.

Figure 29. Schematic of SPF beaded web panel cross-section.

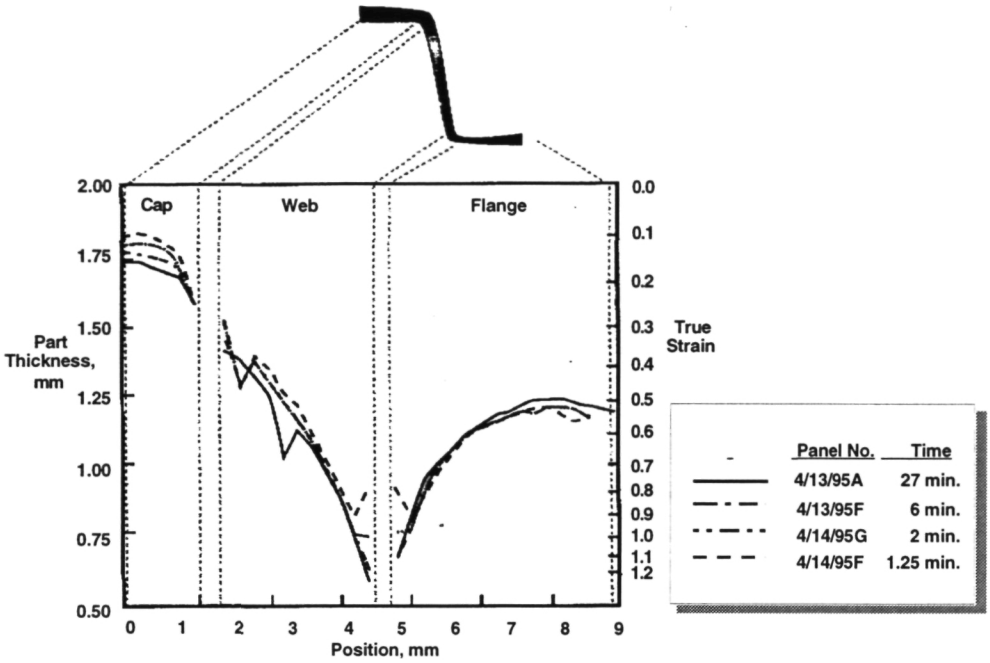

Figure 30. SKY 5083 SPF beaded web stiffener panel thickness profiles and strains after forming.

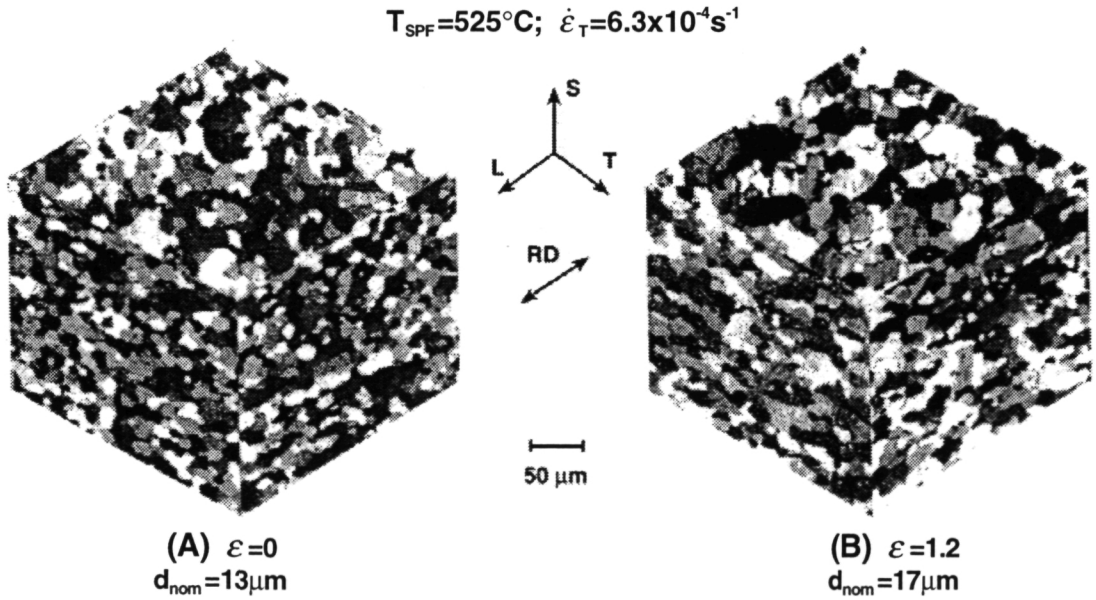

Figure 31. Microstructural coarsening in SKY 5083 during biaxial deformation.

2.3 MULTI-SHEET STRUCTURES

Boeing

2.3.2. Explore multi-sheet SPF concepts for automotive structures.

Prospective multi-sheet automotive applications are being explored through technical exchange meetings among Boeing and GM R&D engineers. Potential components are being categorized as either stiffness/crush critical applications or as part-consolidation applications. However, there are elements of both issues in most parts.

With all of these parts, both part-for-part replacement and part consolidation were considered. Maximum advantage of multi-sheet SPF technology would be achieved by "re-thinking" the entire automobile design, for example, specifying a one-piece, multi-sheet, laser blank welded (LBW) SPF side frame.

2.3.2.1 Explore stiffness/crush applications

Four stiffness/crush applications were explored.

1. **Shock towers:** This is one of the few places an automobile must carry very high loads. A multi-sheet shock tower that incorporates an integral front upper rail has the potential to reduce weight and cost.
2. **Truck/Van floor pans:** The maximum structural advantage of multi-sheet sandwich panels is achieved in areas where small volumes must carry high loads. Truck floor pans (e.g., G-van, M-Van) could benefit from multi-sheet aluminum sandwich structure's good bending performance.
3. **Deck Lids, Hoods and Roof Panels:** These are excellent stiffness critical applications for multi-sheet structures. However, they require much better surface finish than is currently possible with multi-sheet SPF. Therefore, a secondary bonding operation to attach a thin plastic or aluminum skin would likely be necessary.
4. **Seats:** Seats were identified as requiring high strength and stiffness. The application is scheduled for investigation during SPITFIRE-2–5.

2.3.2.2. Explore part consolidation applications

Three parts-consolidation applications were explored.

1. A, B-, C-Pillars and Rails: Many of these parts are currently built-up by resistance spot welding of several sets of stamped sheets. Multi-sheet SPF has the potential to reduce cost by eliminating manufacturing steps.
2. Instrument Panels: These have many attachments and could benefit by the ability of multi-sheet SPF to incorporate fasteners, stiffeners, and attachment bosses. In addition, the multi-sheet construction could potentially help reduce cockpit noise.
3. Others: Additional part-consolidation applications are possible but would require extensive re-design work, for example, floor pans with integral rails and entire side frames.

2.3.2.3 Evaluate structural characteristics of multi-sheet components

The feasibility of LBW SPF multi-sheet panels has been demonstrated. However, further process development is required before structural characterization work can begin. Parts suitable for structural testing may be ready by the end of Boeing's contract with GM (October 27, 1995).

2.3.3. Identify promising multi-sheet structures for further development

Pillars (A-, B-, and C-) were identified as the most promising automotive applications for aluminum multi-sheet SPF. Several concepts for forming generic pillar/rocker/rail structures are shown in Figure 32. It is recommended that GM and Boeing pick one of the identified concepts for further development.

Currently, plans are being made to meet with GM R&D and NASA at Boeing in early August to discuss cost modeling of SPF parts for aerospace applications. Also, a meeting is planned at GM in mid-August to cooperatively choose and begin development of one of the identified concepts.

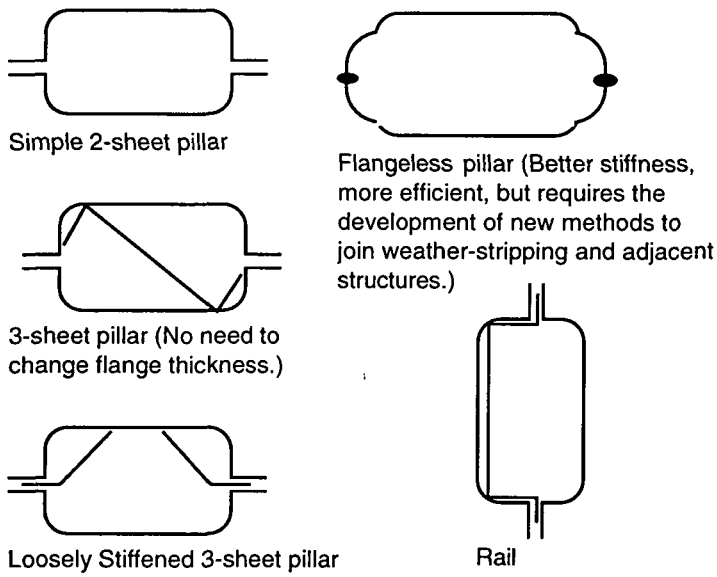

Figure 32. Pillar/rail concepts for multi-sheet aluminum SPF.

TOPIC 3-TOOLING & DESIGN

STATEMENT OF WORK:

This section documents the recent developments in high volume tooling concepts for SPF. The work covering the last period has been specifically focused on evaluating the durability of candidate tooling materials. The first phase of the study consists of screening candidate materials in laboratory tests. Tests are now underway, but no data has yet been produced.

Test methods for evaluating the tribological and durability characteristics of tooling for superplastic forming were identified and will be evaluated in the future. SPF tribological properties and friction coefficients were determined and characterized. Possible wear mechanisms in the high temperature ranges of the SPF process were identified. Based on these results, a new friction tester that more closely simulates SPF will be developed and built for future tests.

The tooling investigation in SPITFIRE-1 indentified the more conventional tooling materials and fabrication techniques as primary. Advanced materials and processes, i.e., composite materials, shall not be the focus of SPITFIRE-2–5. Currently these materials are not cost competitive, but they will be monitored as potential future tooling materials.

General Motors Research and Development Center

3.2.2.2 Assess changes in the quality of selected SPF tooling materials on extended service; 3.2.2.3 Evaluate viability of tooling concepts for extended service application

Currently GM R&D-Metallurgy is evaluating five metallic materials as potential high volume SPF tooling materials: 316 stainless steel, GM 246 nodular cast iron, H13 tool steel, 413.2 cast aluminum, and GM190 cast steel. Initially, these materials are being evaluated under thermal cycling and static loading conditions. For thermal cycling, the 12mm x 200mm x 6mm samples are placed on the testing fixture (Figure 33) and will be evaluated in a 24-hour cycle. They will be heated to 550°C and held for 10 hours and subsequently cooled to room temperature and maintained for 14 hours. This cycle will continue for 30 days, after which the specimens will be measured to see if there is any distortion. These experiments are underway at GM R&D-Metallurgy.

A four-point bend fixture has been designed and constructed to apply a static load to 12mm x 200 mm x 6mm samples (Figure 34). Constant fiber stresses of 1.38MPa and 4.14 MPa will be applied at temperatures between 400°C and 550°C. The strain in the samples will be measured at various times, i.e., 1hr, 10 hr, 100 hr, etc., until noticeable deformation has occurred. These experiments will be initiated later this summer.

3.2.3 Identify promising tooling materials and concepts

In the initial stages of this study, a number of advanced materials were considered as potential high volume production, SPF tooling materials. However, after further investigation, it was determined that conventional tooling materials, i.e., ferrous and aluminum alloys, were more realistic for high volume SPF tooling. The two deterrents for advanced materials were cost and availability. Cast iron or steel only costs about $0.25 to $1.00 per pound, which is well below that

of any advanced material. There is also a wide network of tool and die suppliers that can provide ferrous or aluminum tooling on demand.

Some advanced materials, such as composites and ceramics, do have promise as SPF tool materials because of their properties. Therefore, GM will still monitor these materials as future candidates for evaluation. However, for the immediate future, these materials will not be included in the testing program.

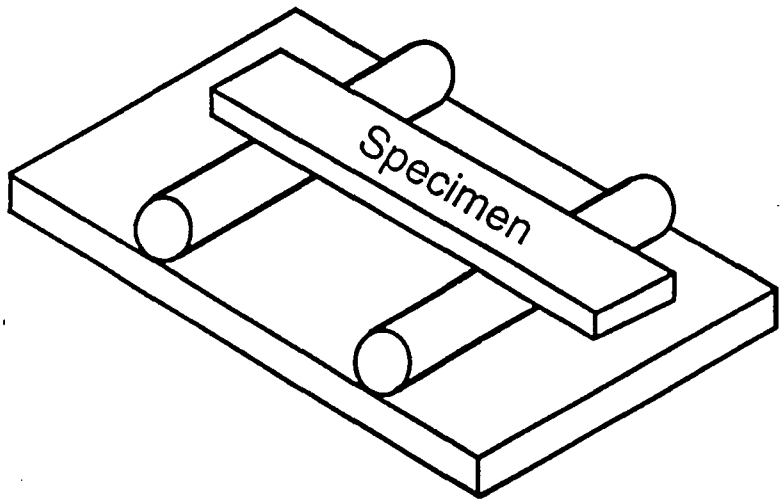

Figure 33. Schematic of the thermal cycling distortion test, in which the specimen is heated during the day and cooled over night for 30 days.

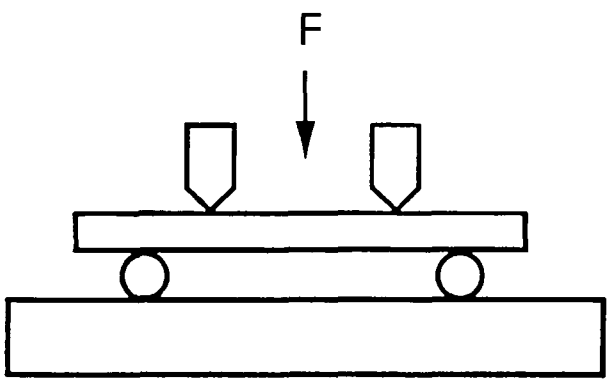

Figure 34. In the modified four-point bend distortion test, a constant load is applied over time and then strain is measured.

3.3 PART DESIGN AND MANUFACTURING

General Motors Research and Development

SPF Component Development

The components to be developed consist of a floor pan, pillar and roof. The statement of work for the design, manufacture, and evaluation of these components are outlined in the SPITFIRE-2–5 proposal. However, due to timing requirements, design of components has already started.

The one-piece floor panel is being designed as a wire-frame model. This panel will replace a number of stamped steel components. Also, a wireframe model of an SPF tool has been developed. Because the width of the tool was greater than that of the largest, commercially available SPF 5083 alloy sheet, the decision was made to fabricate a half-size tool for this part.

The wireframe model of the floor panel tool was converted to a surface model using a GM-proprietary code named SurfSeg. Also, the NC-cutter path was generated using the same code. The current capabilities of SurfSeg and needs for further enhancement for SPF are addressed seperately in the next section.

The design of the roof panel and tooling will start after the floor panel tool is completed. The pillar panel will follow the roof.

Web-Stiffened Channel Study

Open and closed channels will be integrated into the components. Three different configurations were designed, and their finite-element models were created using MARC/MENTAT. The three configurations were built with:

- plain side walls (Case 1),
- narrower side walls, stiffened with 20mm wide webs alternating with 20mm wide plain strips (Case 2), and
- web-stiffened side walls of the same configuration as Case 2, but with the same channel width as Case 1 (Case 3).

The web-stiffened channels simulated the pieces designed and fabricated by LaRC in their investigation. The three-point bending situation was simulated using MARC on the above channels with or without a flat panel closing the channel sections. With the open geometry, the plain-walled channel was found to be significantly superior to the channel in Case 2, which in turn was stiffer than the channel in Case 3. When the channels are closed, however, the ranking changed. The plain channel was the stiffest, followed by those from Case 2 and Case 3.

In the following months, the models will be analyzed with respect to torsional loading and compressive (buckling) mode of loading.

SPF Cost Modeling

In addition to the technological development promised in the SPITFIRE co-operative agreement, the GM team has been paying full attention to the economics of the SPF technology as applied to automobile BIW manufacture. As more knowledge is gained on designing and SPF of various components, the team will develop an economic model for SPF, which will take into

account all important factors, such as material cost, SPF tool cost, capital cost of SPF presses, forming cycle time, manufacture, assembly, etc.

Progress in CAE Development

The desired capabilities of a computer-assisted design (CAD) or engineering (CAE) software which is ideally suited for SPF applications include:

- efficient automatic merging of components into a single SPF part,
- fast and automatic generation of surface from wireframe design data,
- automatic assignment of corner curvatures,
- automatic addition of periodic features such as web-stiffeners,
- efficient modification of designs, and
- automatic generation of numerically-controlled machining (NC) program.

Most of the currently popular CAD software are deficient in many of the capabilities listed above. A GM-proprietary code named SurfSeg has some of the above capabilities and thus forms the basis of a CAD/CAE software dedicated for SPF.

SurfSeg can generate a surface model from the wireframe, assign corner and fillet curvatures, generate a cutter path, or generate a mesh. All these operations could be done by one person. In a traditional CAD/CAE environment, the wireframe and surface models are created by a designer, but the cutter path generation is carried out by an NC programmer. FEM generation and structure analysis belong to yet another specialty. The goal of SurfSeg is to allow one person to do all these operations.

The need for further enhancement of SurfSeg has been identified, and a computer scientist has been assigned to develop necessary algorithms. The new capabilities to be developed include:

- more advanced corner and fillet smoothing algorithms, which can universally apply scientific logic or take user input at selected locations
- automatic generation of binder wrap surface from the part definition and user-selected binder height and peripheral tool dimensions
- prediction of thickness in formed part using a set of approximating assumptions

GM has conducted an intensive benchmark analyses on the MARC code. The findings from this effort include:

- MARC can directly read die surface data in a number of different formats used in commercial CAD software. This capability is deemed critical for SPF simulation and sets MARC apart today from the rest of the nonlinear FEA vendors.
- The contact algorithm along with the rigid-plastic material model implemented in MARC provides faster analysis than other codes; on one large model, MARC outperformed ABAQUS by a factor greater than five.
- Contact chattering and increment splitting did not occur in all cases analyzed, whereas such was common in other software.

- The ability of MARC in accepting a user-input constitutive relationship is a significant advantage in SPF simulation.
- To further enhance the capability of MARC, GM is in the process of reaching an agreement with MARC Research and Analysis Corporation to enter a two-year collaborative work.

With respect to developing accurate constitutive equations for SPF, there has been significant progress in a parallel program under a CRADA with the Pacific Northwest Laboratories. In actual SPF of automobile components, the forming temperature has to be determined so as to provide adequate strength to the part for shape retention without unacceptable increase in the forming cycle time. Therefore, the experimental data base on superplastic properties of a family of 5083-based alloys are being expanded to cover a wide range of temperature and strain rate. Constitutive equations are being developed using both the micro-mechanistic and the experimental mechanics approaches. In the latter approach, simpler, curve-fit equations can be quickly developed from tension test data covering the full range of actual SPF temperatures.

APPENDIX A: TOPIC 1 - ALLOY DEVELOPMENT DELIVERABLES SUMMARY

Time Frame	Deliverable	Responsibility
4 Months	Progress report on baseline structure/property of current 5083 Al alloys (Task 1.1.1).	GM
	Progress report on baseline structure/property data of alternate superplastic Al alloys (Task 1.1.2).	NASA
	Progress report on existing high cooling rate concepts for producing superplastic Al alloys (Task 1.2.1).	GM
9 Months	Progress report on modifications of alloying compositions and TMP treatments for 5000 Al alloys (Tasks 1.1.3 and 1.1.5).	GM
	Progress report on selection of alternate superplastic Al alloys and TMP treatments (Tasks 1.1.4 and 1.1.6).	NASA
	Progress report on development of viable high cooling rate concepts and new casting techniques (Tasks 1.2.2).	GM
12 Months	Final report and biaxially formed components on modified superplastic 5000 Al alloys (Tasks 1.1.1, 1.1.3, 1.1.5 and 1.1.7).	GM
	Final report and biaxially formed components of alternate superplastic Al.alloys (Tasks 1.1.2, 1.1.4, 1.1.6 and 1.1.7).	NASA
	Final report on viable high cooling rate concepts for obtaining superplastic Al alloys (All Tasks in 1.2).	GM

Milestones

- Target SPF properties of 5000 and alternate Al alloys established (1/94).
- Initial 5000 and alternate Al alloy candidates obtained for evaluation (2/94).
- Promising alloy and TMP variants of 5000 and alternate Al alloys selected for further development (12/94).

APPENDIX B: TOPIC 2 - MANUFACTURING PROCESSES DELIVERABLES SUMMARY

Time Frame	Deliverable	Responsibility
4 Months	Progress report on baseline information on existing manufacturing processes (Task 2.1.1).	GM
	Progress report on study of new rapid forming alternatives (Task 2.2.1).	GM
	Progress report on baseline information on multi-sheet structures (Task 2.3.1).	BOE
9 Months	Progress report on evaluation of current component quality (Task 2.1.2).	GM
	Progress report on mechanical forming feasibility (Task 2.2.2).	GM
	Progress report on multi-sheet structures (Tasks 2.3.2 and 2.3.3).	BOE
12 Months	Final report on rapid forming alternatives (Tasks 2.1 and 2.2).	GM
	Final report on multi-sheet structures (Tasks 2.3).	BOE

Milestones

- Mechanical properties and dimensions for SPF component summarized (3/94).
- Influence of manufacturing operating parameters on forming economics determined through the use of the GM DDP model (6/94).
- Uniaxial tests on SPF alloys at temperatures and strain rates outside the nominal SPF regime completed (11/94). (Pending installation of new servohydraulic machine and furnace combination.)

APPENDIX C: TOPIC 3 - TOOLING & DESIGN DELIVERABLES SUMMARY

Time Frame	Deliverable	Responsibility
4 Months	Progress report on baseline tooling technology (Task 3.1.1).	GM
	Progress report on high-volume tooling concepts (Task 3.2.1).	GM
	Progress report on baseline design processes (Task 3.3.1.1 and 3.3.1.2).	GM
9 Months	Progress report on high-volume tool concepts and durability (Tasks 3.1.2 and 3.2.2).	GM
	Progress report on part/tool design using current and new technologies (Tasks 3.3.2 and 3.3.3).	GM
12 Months	Final report on high-volume tool concepts (Tasks 3.1 and 3.2).	GM
	Final report on design concepts (Task 3.3).	GM

Milestones

- Results from the GM DDP and other cost models available on two automotive applications (6/94).
- Development of bench test for tool durability completed (9/94).
- Design optimization completed for an automotive subassembly (11/94).